Diagnostic Applications of Nuclear Medicine: Brain Tumors

17

Giampiero Giovacchini, Mattia Riondato, Elisabetta Giovannini, and Andrea Ciarmiello

Abstract

PET/CT and PET/MR can be used with various radiopharmaceuticals to assess the mechanisms underlying biochemical changes and physiopathology of brain tumors.

Amino acid tracers are frequently used for most clinical questions. These tracers include, among others, [^{11}C]methionine, *L*-3,4-dihydroxy-6[^{18}F]fluorophenylalanine ([^{18}F]FDOPA and O-(2-^{18}F-fluoroethyl)-L-tyrosine (^{18}F-FLT). Amino acid tracers are particularly accurate to distinguish tumor recurrence and radiation necrosis. The role of [^{18}F]FDG, the earliest PET tracer used for diagnosis and monitoring of brain tumors, is being redefined, due to the availability of amino acid tracers. For in vivo prediction of tumor grade, however, [^{18}F]FDG is still more accurate than most amino acid tracers.

Higher baseline values of tracer uptake as well as lower percent changes after therapy in treated patients predict shorter survival – this has been shown for several tracers.

PET/CT and PET/MR can be used after surgery to assess the presence of residual tumor. PET, in combination with MR, is increasingly used for the definition of the tumor volume that has to be irradiated. Identification of the part of the tumor that displays highest metabolic activity can also be used to direct stereotaxic biopsy.

Other tracers have been synthetized to explore different biochemical processes, for example, hypoxia (e.g., [^{18}F]-fluoromisonidazole), DNA synthesis (3-deoxy-3-[^{18}F]-fluorothymidine), and membrane proliferation (radiolabeled choline). However, these tracers have a less established role in clinical practice.

Keywords

Brain tumor • Positron emission tomography/computed tomography (PET/CT) • Positron emission tomography/magnetic resonance (PET/MR)

Glossary

[^{11}C]MET	[^{11}C]methionine
[^{18}F]FDG	2-Deoxy-2-[^{18}F]fluoro-D-glucose
[^{18}F]FDOPA	*L*-3,4-dihydroxy-6-[^{18}F]fluorophenylalanine
^{123}I-IAZA	^{123}I-iodoazomycin arabinoside
^{123}I-IMT	^{123}I-alpha-methyltyrosine, a tyrosine analog transported as L-tyrosine by the neutral amino acid transporter
^{18}F-FAZA	^{18}F-azomycin arabinoside
^{18}F-FES	16α-^{18}F-fluoro-17β-oestradiol

G. Giovacchini • M. Riondato • E. Giovannini • A. Ciarmiello (✉)
Nuclear Medicine Department, S. Andrea Hospital, La Spezia, Italy
e-mail: andrea.ciarmiello@asl5.liguria.it

H.W. Strauss et al. (eds.), *Nuclear Oncology*,
https://doi.org/10.1007/978-3-319-26236-9_9

^{18}F-FET	*O*-(2-^{18}F-Fluoroethyl)-L-Tyrosine, a tyrosine analog
^{18}F-FLT	^{18}F-fluorothymidine
^{18}F-FMAU	^{18}F-2-fluoro-5-methyl-1-beta-d-arabinofuranosyluracil
^{18}F-MISO	^{18}F-fluoromisonidazole
^{64}Cu-ATSM	^{64}Cu-diacetyl-bis(N_4-methylsemicarbazone)
^{99m}Tc-ECD	^{99m}Tc-ethylcisteinate dimer
^{99m}Tc-HMPAO	^{99m}Tc-hexa-methylpropyleneamine oxime
ADC	Apparent diffusion coefficient, a parameter of MR imaging
AJCC	American Joint Committee on Cancer
BBB	Blood–brain barrier
BTV	Biological tumor volume (the extent of tumor based on PET imaging); the combination of GTV and BTV provides the planning target volume for radiation therapy
CBF	Cerebral blood flow
CI	Confidence interval
CMR_{glc}	Cerebral metabolic rate for glucose
CNS	Central nervous system
CSF	Cerebrospinal fluid
CT	X-ray computed tomography
DG	2-Deoxyglucose
DOTA	1,4,7,10-Tetra-azacyclododecane-1,4,7,10-tetraacetic acid
DOTANOC	DOTA-1-Nal^3-octreotide
DOTATATE	DOTA- Tyr^3-octreotate
DOTATOC	DOTA-octreotate
DTPA	Diethylenetriaminepentaacetic acid
DWI	Diffusion-weighted imaging, an MR imaging technique
EGFR	Epidermal growth factor receptor; the mutated form EGFRvIII plays a prominent role in tumorigenesis and pro-angiogenic signaling
FLAIR	Fluid-attenuated inversion recovery, an MR imaging technique
GBM	Glioblastoma multiforme
GTV	Gross tumor voume (the extent of the tumor on morphologic imaging)
IDH	Isocitrate dehydrogenase; mutations of this enzyme occur more frequently in oligodendroglial and astrocytic tumors
KPS	Karnofsky performance score
LAT1	L-type amino acid transporter 1
M	Metastasis status according to the AJCC/UICC TNM staging system
MDR1	Multidrug resistance gene 1, a characteristic associated with aggressive tumors; this gene encodes for P-glyoprotein
MGMT	Methyl guanine DNA methyl transferase, a DNA repair enzyme; methylation of MGMT promoter is associated with increased overall survival
MIB-1	Marker of cell proliferation used for stratification of grades of brain tumors
MoAb	Monoclonal antibody
MPNST	Malignant peripheral nerve sheath tumor
MR	Magnetic resonance
MRI	Magnetic resonance imaging
N	Lymph node status according to the AJCC/UICC TNM staging system
PET	Positron emission tomography
PET/CT	Positron emission tomography/computed tomography
PET/MR	Positron emission tomography/magnetic resonance
PI3K	Phosphatidylinositol 3-kinase
PNET	Primitive neuroectodermic tumor
pRIT	Pretargeting radioimmunotherapy
PTEN	Phosphatase and tensin homolog is a tumor suppressor; PTEN deletions indicate a poor prognosis
RIT	Radioimmunotherapy

ROC	Receiver operating characteristic, a statistical analysis to assess the performance of a binary classifier
ROI	Region of interest
SPECT	Single photon emission computed tomography
SPECT/CT	Single photon emission computed tomography/computed tomography
SST	Somatostatin
SSTR	Somatostatin receptors
SUV	Standardized uptake value
T	Tumor status according to the AJCC/UICC TNM staging system
T/N	Ratio of tumor uptake to normal brain uptake
TBR	Tumor-to-background ratio
TNM	AJCC/UICC staging system based on parameters "T" (tumor status), "N" (lymph node status), and "M" (distant metastasis status)
TP53	Tumor protein p53, also known as cellular tumor antigen p53, phosphoprotein p53, tumor suppressor p53, antigen NY-CO-13, or transformation-related protein 53 (TRP53)
UICC	Union Internationale Contre le Cancer (International Union Against Cancer)
VEGF	Vascular endothelial growth factor
VOI	Volume of interest
WHO	World Health Organization

Contents

Primary brain tumors are a heterogeneous group of neoplasms, each with its own biology, prognosis, and treatment. Among primary brain tumors, gliomas constitute the most frequent pathologic finding, being characterized by distinct histologic patterns and grades that are predictive of tumor invasiveness and patient survival. In this chapter we will review the main features of neoplasms of the central nervous system (CNS), and we will focus on the use of positron emission tomography (PET) and single-photon emission computed tomography (SPECT) as well as of hybrid techniques, particularly PET with computed tomography (PET/CT) and PET with magnetic resonance (PET/MR) with various radiopharmaceuticals for the diagnosis, treatment, and follow-up of brain tumors. Even though nowadays all PET tomographs are either PET/CT or PET/MR tomographs, the term PET will be used often either to contrast CT or MR studies or to refer to old studies that were performed with stand-alone PET tomographs.

Epidemiology of Brain Tumors

Many different organizations track the incidence of gliomas. This can be done using data collected through government cancer surveillance

(i.e., statewide or countrywide cancer registries) [1] or through the use of health system records [2]. Incidence rates of glioma vary significantly by histologic type, age at diagnosis, gender, race, and country. Overall age-adjusted incidence rates range from 4.67 to 5.73 per 100,000 persons. Age-adjusted incidence of glioblastoma, the most common and most deadly glioma subtype in adults, ranges from 0.59 to 3.69 per 100,000 persons [3, 4]. Although brain tumors are more frequent in adult subjects, they can occur in pediatric patients and adolescents as well. However, age and gender distribution vary accordingly to histotype. Meningiomas are more common in females than in males with a 3:2 ratio, while gliomas are slightly more common in men. The age-adjusted incidence rates of brain tumors tend to be highest in developed, industrial countries. However, the lower incidence of brain tumors in developing countries may also be attributed to decreased diagnosis [5].

Staging and Prognostic Stratification

The American Joint Committee on Cancer (AJCC) in agreement with the World Health Organization (WHO) classification of tumors of the CNS was updated a few years ago [6]. On the basis of histological origin, the WHO classification identifies six types of CNS neoplasms (Table 1): (1) tumors of the neuroepithelial tissue, (2) tumors of the cranial and paraspinal nerves, (3) tumors of the meninges (meningiomas), (4) lymphomas and hematopoietic neoplasms, (5) germ cell tumors, and (6) tumors of the sellar region. In addition to these primary CNS tumors, metastatic tumors need to be considered as well. Most neuroepithelial tumors are derived from glial cells and therefore are termed gliomas. There are three types of gliomas, namely, astrocytomas, oligodendrogliomas, and ependymomas. The category of astrocytomas is included in the glioblastoma. However, some tumors, such as the medulloblastoma, derive from neurons. In this chapter, we will focus particular attention to the distinction between low-grade and high-grade gliomas and briefly mention meningiomas.

CNS tumors do not currently have TNM designation [6]. Attempts at developing a TNM-based classification and staging system for CNS tumors have been disappointing. There are multiple reasons for this. (1) Tumor size is significantly less relevant than tumor histology and tumor grading (Table 2). Thus, the T classification is less pertinent than the biologic nature of the tumor itself. (2) Because the brain and spinal cord have no lymphatics, the N classification does not apply. (3) An M classification is not pertinent to the majority of CNS tumors, because they have the tendency to recur locally and they virtually never disseminate at distance.

Based on the histological features, CNS tumors are divided into low-grade and high-grade tumors. Grading is based on the degree of nuclear atypia, mitosis, microvascular proliferation, and necrosis. Grading is clinically important because prognosis worsens as tumor grading increases. Tumor grade is determined by multiple histological sampling of tumor tissue. Grading becomes unreliable in treated tumors because blood–brain barrier (BBB) damage and necrosis also can result from the formation of reactive tissue after therapy [7].

Low-grade gliomas are grade I and II, while high-grade gliomas are grade III and IV. Since histological features may vary within different areas of the same tumors, the most malignant region determines the grade of the tumor. Grade III astrocytomas are commonly referred to as anaplastic astrocytomas. Glioblastoma, a grade IV glioma, is the most malignant as well as the most common form of gliomas, accounting for about 50% of all gliomas [8]. All glioblastomas can be divided into two subtypes based on the presence or absence of a precursor lesion of a lower grade. Primary high-grade glioblastomas develop more commonly in subjects younger than 45 years, while secondary glioblastomas that progressed from low-grade gliomas occur more frequently in older subjects (>60 years). Primary glioblastoma is the most common type (>90%) and diagnosed as a de novo lesion without progression from a lower-grade tumor in older patients. Secondary glioblastomas develop through progression from a low-grade diffuse astrocytoma or anaplastic astrocytoma and present in younger patients [9].

Table 1 The 2010 AJCC classification of tumors of the CNS (Adapted from Ref. [6])

(1) *Tumors of neuroepithelial tissue*	
Astrocytic tumors	
Pilocytic astrocytoma	9421/1[a]
Pilomyxoid astrocytoma	*9425/3*[b]
Subependymal giant cell astrocytoma	9384/1
Pleomorphic xanthoastrocytoma	9424/3
Diffuse astrocytoma	9400/3
Fibrillary astrocytoma	9420/3
Gemistocytic astrocytoma	9411/3
Protoplasmic astrocytoma	9410/3
Anaplastic astrocytoma	9401/3
Glioblastoma	9440/3
Giant cell glioblastoma	9441/3
Gliosarcoma	9442/3
Gliomatosis cerebri	9381/3
Oligodendroglial tumors	
Oligodendroglioma	9450/3
Anaplastic oligodendroglioma	9451/3
Oligoastrocytic tumors	
Oligoastrocytoma	9382/3
Anaplastic oligoastrocytoma	9382/3
Ependymal tumors	
Subependymoma	9383/1
Myxopapillary ependymoma	9394/1
Ependymoma	9391/3
Cellular	9391/3
Papillary	9393/3
Clear cell	9391/3
Tanycytic	9391/3
Anaplastic ependymoma	9392/3
Choroid plexus tumors	
Choroid plexus papilloma	9390/0
Atypical choroid plexus papilloma	*9390/1*
Choroid plexus carcinoma	9390/3
Other neuroepithelial tumors	
Astroblastoma	9430/3
Chordoid glioma of the third ventricle	9444/1
Angiocentric glioma	9431/1
Neuronal and mixed neuronal-glial tumors	
Dysplastic gangliocytoma of cerebellum	9493/0
Desmoplastic infantile astrocytoma/ganglioglioma	9412/1
Dysembryoplastic neuroepithelial tumor	9413/0
Gangliocytoma	9492/0
Ganglioglioma	9505/1
Anaplastic ganglioglioma	9505/3
Central neurocytoma	9506/1
Extraventricular neurocytoma	*9506/1*[b]
Cerebellar liponeurocytoma	*9506/1*[b]
Papillary glioneuronal tumor	*9509/1*[b]
Rosette-forming glioneuronal tumor of the fourth ventricle	*9509/1*[b]
Paraganglioma	8680/1
Tumors of the pineal region	
Pineocytoma	9361/1
Pineal parenchymal tumor of intermediate differentiation	9362/3
Pineoblastoma	9362/3
Papillary tumor of the pineal region	*9395/3*[b]
Embryonal tumors	
Medulloblastoma	9470/3
Desmoplastic/nodular medulloblastoma	9471/3
Medulloblastoma with extensive nodularity	*9471/3*[b]
Anaplastic medulloblastoma	*9474/3*[b]
Large cell medulloblastoma	9474/3
CNS primitive neuroectodermal tumor	9473/3
CNS neuroblastoma	9500/3
CNS ganglioneuroblastoma	9490/3
Medulloepithelioma	9501/3
Ependymoblastoma	9392/3
Atypical teratoid/rhabdoid tumor	9508/3
(2) *Tumors of cranial and paraspinal nerves*	
Schwannoma (neurilemoma, neurinoma)	9560/0
Cellular	9560/0
Plexiform	9560/0
Melanotic	9560/0
Neurofibroma	9540/0
Plexiform	9550/0
Perineurioma	
Perineurinoma, NOS	9571/0
Malignant perineurinoma	9571/3
Malignant peripheral nerve sheath tumor (MPNST)	
Epithelioid MPNST	9540/3
MPNST with mesenchymal differentiation	9540/3
Melanotic MPNST	9540/3
(3) *Tumors of the meninges*	
Tumors of meningothelial cells	
Meningioma	9530/0
Meningothelial	9531/0
Fibrous (fibroblastic)	9532/0
Transitional (mixed)	9537/0
Psammomatous	9533/0
Angiomatous	9534/0
Microcystic	9530/0
Secretory	9530/0
Lymphoplasmacyte-rich	9530/0

(*continued*)

Table 1 (continued)

Metaplastic	9530/0
Chordoid	9538/1
Clear cell	9538/1
Atypical	9539/1
Papillary	9538/3
Rhabdoid	9538/3
Anaplastic (malignant)	9530/3
Mesenchymal tumors	
Lipoma	8850/0
Angiolipoma	8861/0
Hibernoma	8880/0
Liposarcoma	8850/3
Solitary fibrous tumor	8815/0
Fibrosarcoma	8810/3
Malignant fibrous histiocytoma	8830/3
Leiomyoma	8890/0
Leiomyosarcoma	8890/3
Rhabdomyoma	8900/0
Rhabdomyosarcoma	8900/3
Chondroma	9220/0
Chondrosarcoma	9220/3
Osteoma	9180/0
Osteosarcoma	9180/3
Osteochondroma	9210/0
Hemangioma	9120/0
Epithelioid hemangioendothelioma	9133/1
Hemangiopericytoma	9150/1
Anaplastic hemangiopericytoma	9150/3
Angiosarcoma	9120/3
Kaposi sarcoma	9140/3
Ewing sarcoma – PNET	9364/3
Primary melanocytic lesions	
Diffuse melanocytosis	8728/0
Melanocytoma	8728/1
Malignant melanoma	8720/3
Meningeal melanomatosis	8728/3
Other neoplasms related to the meninges	
Hemangioblastoma	9161/1
(4) *Lymphomas and hematopoietic neoplasms*	
Malignant lymphomas	9590/3
Plasmacytoma	9731/3
Granulocytic sarcoma	9930/3
(5) *Germ cell tumors*	
Germinoma	9064/3
Embryonal carcinoma	9070/3
Yolk sac tumor	9071/3
Choriocarcinoma	9100/3
Teratoma	9080/1
Mature	9080/0
Immature	9080/3
Teratoma with malignant transformation	9084/3
Mixed germ cell tumor	9085/3
(6) *Tumors of the sellar region*	
Craniopharyngioma	9350/1
Adamantinomatous	9351/1
Papillary	9352/1
Granular cell tumor	9582/0
Pituicytoma	9432/1[b]
Spindle cell oncocytoma of the adenohypophysis	8291/0[b]

(*continued*)

[a]Morphology code of the International Classification of Diseases for Oncology (ICO-O) (614A) and the Systematized Nomenclature of Medicine (http://snomed.org). Behavior is coded /0 for benign tumors, /3 for malignant tumors, and /1 for borderline or uncertain behavior

[b]The italicized numbers are provisional codes proposed for the fourth edition of ICD-O. While they are expected to be incorporated into the next ICD-O edition, they currently remain subject to change

Glioblastomas are highly aggressive tumors that are generally resistant to treatment. Average survival is less than 1 year from diagnosis. Glioblastomas are characterized by hypercellular anaplastic glioma cells with marked mitotic activity as well as necrosis and endothelial proliferation. Neoplastic cells frequently reveal pleomorphism showing different histologic features such as small homogeneous cells with scant cytoplasm, fibrillary-shaped cells, multinucleated giant cells, and cells with pleomorphic nuclei and cytoplasm [10]. Because of such cellular pleomorphism, the tumor is often referred to as glioblastoma multiforme (GBM) [10]. Histologic features in glioblastomas are associated with clinical outcome: greater necrotic component is associated with poor survival, while greater oligodendroglial component is predictive of longer survival [11].

Genetic Predisposition and Underlying Molecular Biology Changes

The traditional classification of brain tumors of the WHO grades II–IV is based on histological features of a heterogeneous population of tumors with varying prognoses and treatments. Histologic visual criteria may be prone to errors, and interpreting

Table 2 WHO grades of CNS tumors

	I	II	III	IV		I	II	III	IV
Astrocytic tumors					Central neurocytoma		●		
Subependymal giant cell astrocytoma	●				Extraventricular neurocytoma		●		
Pilocytic astrocytoma	●				Cerebellar liponeurocytoma		●		
Pilomyxoid astrocytoma		●			Paraganglioma of the spinal cord	●			
Diffuse astrocytoma		●			Papillary glioneuronal tumor	●			
Pleomorphic xanthoastrocytoma		●			Rosette-forming glioneuronal tumor of the fourth ventricle	●			
Anaplastic astrocytoma			●		Pineal tumors				
Glioblastoma				●	Pineocytoma	●			
Giant cell glioblastoma				●	Pineal parenchymal tumor of intermediate differentiation		●	●	
Gliosarcoma				●	Pineoblastoma				●
Oligodendroglial tumors					Papillary tumor of the pineal region		●	●	
Oligodendroglioma		●			Embryonal tumors				
Anaplastic oligodendroglioma			●		Medulloblastoma				●
Oligoastrocytic tumors					CNS primitive neuroectodermal tumor (PNET)				●
Oligoastrocytoma		●			Atypical teratoid/rhabdoid tumor				●
Anaplastic oligoastrocytoma			●		Tumors of the cranial and paraspinal nerves				
Ependymal tumors					Schwannoma	●			
Subependymoma		●			Neurofibroma	●			
Myxopapillary ependymoma		●			Perineurioma	●	●	●	
Ependymoma			●		Malignant peripheral nerve sheath tumor (MPNST)		●	●	●
Anaplastic ependymoma				●	Meningeal tumors				
Choroid plexus tumors					Meningioma	●			
Choroid plexus papilloma		●			Atypical meningioma		●		
Atypical choroid plexus papilloma			●		Anaplastic/malignant meningioma			●	
Choroid plexus carcinoma				●	Hemangiopericytoma		●		
Other neuroepithelial tumors					Anaplastic hemangiopericytoma			●	
Angiocentric glioma		●			Hemangioblastoma	●			
Chordoid glioma of the third ventricle			●		Tumors of the sellar region				
Neuronal and mixed neuronal-glial tumors					Craniopharyngioma	●			
Gangliocytoma		●			Granular cell tumor of the neurohypophysis	●			
Ganglioglioma		●			Pituicytoma	●			
Anaplastic ganglioglioma				●	Spindle cell oncocytoma of the adenohypophysis	●			
Desmoplastic infantile astrocytoma and ganglioglioma		●							
Dysembryoplastic neuroepithelial tumor		●							

Adapted from Ref. [6]

cellularity is not always possible due to the histological heterogeneity of the tumor. Over the last decade, research efforts have resulted in a better understanding of the molecular basis of glioma formation as well as the genetic alterations commonly identified in gliomas [9].

The discovery and characterization of the isocitrate dehydrogenase (IDH) 1 and 2 mutations in brain tumors that occurred in the last 6 years is a major achievement. IDH1 and IDH2 mutations occur more frequently in oligodendroglial and astrocytic tumors and less frequently in GBMs. IDH mutant gliomas have indeed a better prognosis in comparison to IDH wild-type gliomas [12]. Whether mutations in IDH result in a loss of tumor suppressor function or act as an oncogene remains a source of debate. It has been hypothesized that the effects of the IDH mutant enzyme's product, 2-hydroxyglutarate, change a cell's methylation profile and alter cell telomere length and gene expression. The effects of IDH mutations also produce decreased cytoplasmic levels of alpha-ketoglutarate and nicotinamide adenine dinucleotide phosphate oxidase that may in turn stabilize hypoxia-inducible factor 1-α facilitating cellular proliferation [13].

The evolution of a recurrent high-grade glioblastoma is more rapid than a primary high-grade glioblastoma. In the pathway to secondary high-grade glioblastoma, TP53 mutations are the most frequent and earliest detectable genetic alterations, already present in 60% of precursor low-grade astrocytomas [14]. On the contrary, unbalanced translocation of chromosomes 1 and 19 with deletion of the 1p arm and the 19q arm is found in almost 70% of histologically defined oligodendrogliomas. 1p/19q codeletions and TP53 mutations are relatively exclusive of one another, supporting the argument of two separate lineages that can be identified on a molecular basis to supplement histological diagnosis. A 1p/19q codeletion is associated with improved prognosis in low-grade gliomas and it is predictive of improved outcomes with chemotherapy and radiation [15].

The DNA repair enzyme O_6-methyl-guanine-DNA methyltransferase (MGMT) status repairs O^6 alkyl guanine adducts. The repair enzyme mechanism interferes with the overlapping effect of drug, which alkylates at the O_6 position of guanine. Methylation of the promoter of the MGMT gene results in silencing of gene transcription, so that the effect of temozolomide is enhanced. MGMT promoter methylation was identified in 36% of the overall population of glioma series studied, which demonstrated the presence of the mutation improves the effect of temozolomide and ultimately increases overall survival regardless of treatment arm [9, 16]. Numerous trials have shown that MGMT promoter methylation is a prognostic marker associated with improved survival. MGMT promoter methylation can be associated with 1p19q codeletions as well as IDH mutations suggesting it may be an epiphenomenon related to these or other factors that result in improved survival [9, 16].

The epidermal growth factor receptor (EGFR) is a transmembrane receptor in the receptor tyrosine kinase (RTK), phosphatase and tensin homolog, and phosphatidylinositol 3-kinnase (PI3K) cell proliferation pathway. EGFR*vIII*, a mutated form of EGFR, plays a prominent role in tumorigenesis of glioblastoma, but the underlying mechanisms have remained elusive. EGFR*vIII* amplification can lead to increased downstream activity resulting in proangiogenic signaling, increased proliferation, increased tumor cell survival, and migration [17]. EGFR*vIII* amplifications have been reported in approximately 40% of primary glioblastomas. EGFR*vIII* amplification has been reported to be a predictor of poor survival; however, other studies have failed to show this effect. Studies have reported that EGFR*vIII* amplification can predict response to tyrosine kinase inhibitors, especially when PTEN expression is preserved [17, 18].

Phosphatase and tensin homolog (PTEN) is a tumor suppressor gene expressing a protein involved in the same RTK/PTEN/PI3K cell proliferation pathway as EGFR. PTEN mutations are estimated to occur in 15–40% of primary glioblastomas, but up to 80% of glioblastomas have loss of chromosome 10q in the region where PTEN is located (10q23). Chromosome 10q loss, PTEN mutations, and EGFR amplifications are frequently seen together in the small cell phenotype of glioblastoma. PTEN deletions have been

reported to be a poor prognostic factor for pediatric glioblastomas; however, this has not been found true in adult patients [17].

Contrary to other tumors, environmental factors do not play a major role in the development of brain tumors.

Clinical Presentation

Symptoms of brain tumors depend on the location, size, and rate of growth of the tumor. High-grade, fast-growing tumors have early symptom onset, while slow-growing, small-sized tumors may remain asymptomatic for many years, especially if they are located in cerebral mute areas, such as the frontal lobe. In these cases, brain neoplasms can be an incidental finding at CT or MR imaging.

Symptoms can be either focal or generalized and appear in a late phase. Generalized symptoms reflect increased intracranial pressure. The most common symptom is headache. Typically, the headache is diffuse, but it may affect only one side, frequently reflecting the site of the tumor. Generally, headache is more intense on awakening in the morning and responds poorly to analgesics; it wanes spontaneously after few hours. Rarely, headache is throbbing and mimicking migraine. Nausea, vomiting, and sixth-nerve palsy are less common.

Focal symptoms or signs take place when the neoplasm compresses the nearby cerebral parenchyma. They can be motor, sensory, or sensory motor. Aphasia is typical of frontal lobe involvement, ataxia is typical of cerebellar involvement, and diplopia occurs with optic nerve gliomas.

Seizures occur at variable degree in brain tumor patients, being more frequent in low-grade tumors. Typically, the seizures are focal but they may become generalized and cause loss of consciousness.

Prognosis

In addition to the previously mentioned genetic factors, there are other prognostic factors for brain tumors (Table 3).

Table 3 Prognostic factors in CNS tumors

Histology
Pathologic grade
Presence and extent of necrosis
Presence of gemistocytes
Proliferative fraction (Ki-67)
Presence of oligodendroglial component
Presence of cells in mitosis and endothelial proliferation
Age of patient
Functional neurological status
Karnofsky Performance Scale
Extent of resection
Biopsy, subtotal, radical removal
Tumor spread
Presence of local spread
Molecular aspects
Isocitrate dehydrogenase IDH1 and IDH2 mutations (protective factors)
1p/19q codeletion (protective factor)
O_6-methyl-guanine-DNA methyltransferase methylation (protective factor)
TP53 mutations (risk factors)
Epidermal growth factor receptor amplification (risk factor)
Phosphatase and tensin homolog mutations (risk factor)

Tumor histology. Histology is by far the most important variable affecting prognosis, and in many cases it determines the treatment modalities that are employed. Prognosis is worst with highest grade. The latest WHO classification system has combined tumor nomenclature with an associated grading system so that the actual histological diagnosis directly correlates with the histological grade of the tumor. The most common histologies for brain and spinal cord tumors are given in Tables 1 and 2, along with the tumor grade for each different diagnostic category.

Age. Most retrospective outcome studies of brain tumor therapy show that older age at the time of diagnosis is a powerful predictor of poor outcome [5, 19]. This fact holds true for the gliomas, which are the most common primary brain tumors, and for most other tumors that affect the adult population, including most metastatic tumors to the brain. There are, however, some childhood tumors that have a very poor prognosis,

are inherently high grade, and rapidly progress to a fatal outcome. Some metastatic tumors, such as melanoma, occur in younger patients and also violate this general statement with regard to the specific effect of age on prognosis.

Extent of tumor resection. In patients who are treated surgically for tumors of the CNS, the extent of resection is often closely correlated with the outcome. This is a less powerful predictor than tumor histology or age, but most retrospective studies confirm that the extent of removal is positively correlated with survival. For this reason, the documentation of whether a surgical tumor removal is "gross total," "subtotal," or "biopsy only" is useful in determining future therapy and prognosis.

Tumor location. Because of the differential importance of various areas of the brain, the location of a given tumor affecting the brain can have a major impact on the functional outcome, survival, and type of therapy.

Functional neurologic status. Another important prognostic factor in most retrospective studies of CNS tumors is the functional neurologic status of the patient at the time of diagnosis [11]. This has been estimated traditionally using the Karnofsky Performance Scale, which is reproducible, it is well known by most clinicians, and it is in common use for stratification of patients entering clinical trials for the treatment of brain tumors. The outcome and prognosis of patients correlate well with functional neurological status.

Metastatic spread. Tumors affecting the CNS rarely develop extraneural metastases because of inherent biologic characteristics of these tumors and because the brain does not have a well-developed lymphatic drainage system. In addition, many patients with tumors of the CNS have a short life expectancy, which further limits the likelihood of metastatic spread. Certain tumors do spread through cerebrospinal fluid (CSF) pathways, and such spread has a major impact on survival. Dissemination through the CSF pathway is a hallmark of certain childhood tumors, e.g., primitive neuroectodermal tumors, many of which carry a poor prognosis; this event, however, is rarely seen in adult patients with the more common CNS tumors. Primary lymphomas of the CNS may spread along the craniospinal axis and sometimes exhibit intraocular dissemination.

Clinical Applications

Before entering into the issues of PET and SPECT imaging of brain tumors, the clinical situations in which PET/SPECT may be useful are described in Table 4:

1. *Diagnosis*. CNS masses may be incidental findings on MR or CT examinations performed as part of diagnostic staging for non-CNS pathology or following neuroradiological examinations performed for neurological or psychiatric symptoms. In most cases, morphologic assessment by MR imaging is often the first step toward diagnosis of primary brain tumor, allowing the precise assessment of tumor size, margins, mass effect, and the presence or absence of contrast enhancement. However, CT and MR lack specificity and do not allow determination of tumor metabolism and activity. PET may be useful to reinforce the diagnostic hypothesis and to address other issues that are important for presurgical evaluation.
2. In vivo *tumor grading*: Grading is obtained following histological analysis of stereotactic

Table 4 Clinical indications to SPECT or PET imaging in gliomas

Pre-therapy
1. Diagnosis
2. Noninvasive tumor grading
3. Guidance for stereotactic biopsy
4. Surgical planning
5. Identification of metabolically active tumor (or biological target volume, BTV) for radiotherapy planning
6. Evaluation of multidrug resistance
Post-therapy
1. Identification of residual tumor
2. Differential diagnosis between tumor recurrence and radiation necrosis
3. Evaluation of response to therapy
4. Prediction of survival

biopsy or of the surgical specimen, if biopsy is not possible. Thus, it would be desirable to predict tumor grade noninvasively with brain imaging or to use an imaging technique to guide biopsy to the areas that are more likely to be of higher grade.

3. *Guidance for stereotactic biopsy.* A typical feature of gliomas is the variability in histological grade that can occur within the same tumor. This is particularly common in high-grade tumors, which generally evolve from low-grade forms. More than 60% of tumors contain both low-grade and high-grade features. As a consequence, sampling errors on stereotactic biopsy are a matter of particular concern. MR and CT do not provide sufficiently accurate information for distinguishing low-grade from high-grade areas. Whether or not PET can be used for guiding biopsy sampling has been addressed in various studies.
4. *Surgical planning*. MR imaging may underestimate the tumor extent in cerebral gliomas. In fact, margins of the abnormal MR lesion in the autopsy specimens of brains affected by gliomas may have viable tumor cells on histopathological examination. Accurate delineation of tumor extent is critical for a complete resection and for localizing metabolically active areas within the tumor in case of a partial resection.
5. *Radiotherapy planning*. Tumor delineation is also important to define the tumor volume that must be irradiated for therapeutic purposes. Adjuvant radiation therapy improves tumor control and is therefore carried out in all tumor patients. Inaccurate tumor delineation with persistence of viable tumor cells beyond the target area (i.e., geographic misses) is a major cause of treatment failure.

   Radiotherapy planning volume is traditionally based on MR. The target volume defined on the basis of morphological imaging is referred to as gross tumor volume (GTV). One of the most important limitations in the application of image-guided radiotherapy consists in the failure to define the tumor extension precisely, which can be attributed to nonspecific changes of MR after surgery or radiation therapy. Thus, PET has been used to identify the metabolically active brain areas. The metabolically active volume, as identified by PET, is referred to as biological target volume (BTV). The combination of GTV and BTV provides the ultimate planning target volume (PTV).
6. *Differentiation of tumor recurrence* versus *radiation injury.* This is currently the most common indication for a PET study. Radiotherapy is associated with a risk of radiation necrosis, especially in the case of tridimensional, conformal treatments that deliver high local doses to small volumes. The occurrence of necrosis is difficult to predict, and it is necessary to differentiate it from tumor recurrence. Radiotherapy-induced injury of the BBB and brain tissue causes edema, so that contrast enhancement may be evident on both CT and MR. This is a potentially confounding factor, because tumor recurrence is also characterized by contrast enhancement. This typically occurs for high-grade gliomas that invade cerebral vessels, thereby increasing BBB permeability. Thus, the observation of contrast enhancement on CT and MR requires further differential diagnosis.
7. *Assessment of response to therapy.* The majority of non-CNS cancers are responsive to some lines of chemotherapy, and the evaluation of response to therapy is a cornerstone of imaging in oncology. Instead, CNS tumors respond poorly to traditional chemotherapies, and metabolic changes induced by chemotherapy are not routinely evaluated. SPECT and PET studies were performed to assess the biological basis of the poor chemosensitivity of gliomas to most common chemotherapy drugs. Nevertheless, the development of some effective CNS chemotherapy agents, such as temozolomide, and, more recently, of antiangiogenic drugs, such as bevacizumab, has renewed interest in assessing the response to treatment. PET was also used in the past to address the effect on cerebral blood flow and glucose metabolism in response to dexamethasone, which is used to reduce edema and to alleviate neurological symptoms.

8. *Prognostic stratification*. Metabolic pattern as assessed by PET may be useful to predict the behavior of brain tumors. Such prognostic information may be obtained at any time point, i.e., initial staging, response to therapy, and restaging.

This classification of clinical indications for brain tumor imaging is "problem oriented." Not always is a PET scan requested to address all these issues, and some of them are strictly correlated. Using temporal criteria in relation to the main therapeutic events and very similarly to what is done in general oncology, PET scans are indicated in patients with brain tumors:

1. For initial staging
2. After surgery for the evaluation of residual mass
3. For restaging, when suspicious of recurrence or for differential diagnosis from radiation necrosis
4. For the evaluation of response to therapy

Prognostic information can be obtained with appropriate study designs at any time point.

However, tumor recurrence versus radiation necrosis is the typical restaging situation.

Overall Performance of Diagnostic Imaging Other Than Nuclear Medicine

CT is often the first modality employed in a patient presenting with a brain tumor, but MR is the reference imaging modality in brain tumor patients. The role of CT is largely confined to emergent imaging in the detection of hemorrhage, herniation, and hydrocephalus; however, the detection of mass effect from brain tumors and calcification within brain tumors, such as oligodendrogliomas or meningiomas, can have diagnostic relevance [17].

MR sequences exploring morphological features play a major role in the evaluation of and treatment planning of brain tumors. Standard sequences performed utilizing spin-echo techniques include T2 fluid-attenuated inversion recovery (FLAIR), pre-gadolinium T1, and post-gadolinium T1. These sequences are preferably performed in at least two orthogonal planes or obtained with a three-dimensional (3D) sequence that is reformatted into orthogonal planes (i.e., 3D T2 FLAIR). High-resolution isovolumetric sequences such as high-resolution 3D T2 sequences and post-gadolinium T1 spoiled gradient recalled acquisition or similar sequences are generally performed preoperatively with fiducials in place for use with intraoperative navigational software. Similarly, post-gadolinium T1 sequences are performed with a stereotactic head frame in place prior to stereotactic radiosurgery [20]. High-resolution 3D T2* gradient echo sequences, such as susceptibility weighted imaging, are also routinely performed. These susceptibility sensitive sequences are very sensitive to blood degradation products and calcification and may be helpful to depict post-radiotherapy micro-hemorrhages [17].

The primary roles of structural MR in initial brain tumor evaluation include determining the location of the lesion (i.e., intra-axial vs. extra-axial); establishing the specific location within the brain for treatment/biopsy planning; evaluating mass effect on the brain, ventricular system, and vasculature; and suggesting a possible diagnosis. Establishing the diagnosis of a specific tumor type can be challenging, but often the correct diagnosis can be limited to a short list of likely possibilities. Contrast enhancement indicates local breakdown of the blood–brain barrier and is a key feature seen in many brain tumors and other mass lesions. Within gliomas, contrast enhancement is generally considered to be associated with a high-grade tumor although certain low-grade gliomas, such as pilocytic astrocytomas in children, generally show contrast enhancement and certain high-grade gliomas may not enhance. Peritumoral edema is generally T2/FLAIR hyperintense signal abnormality surrounding the main mass lesion. This may in some instances, such as with metastasis, represent predominately vasogenic edema surrounding the lesion. However, with gliomas the peritumoral edema generally also represents infiltrative edema caused by tumor cells infiltrating into the regions of non-enhancing T2/FLAIR signal abnormality. The number of lesions is an important factor to consider

as a large number of lesions may signify certain pathologies, such as metastases. However, metastasis can be solitary, and demyelinating lesions or cerebral abscesses can also mimic tumor. Other potentially discriminating features to note include a cyst and mural nodule morphology (seen with the lower-grade tumor hemangioblastoma, pilocytic astrocytoma, ganglioglioma, and pleomorphic xanthoastrocytoma), calcification (generally seen with oligodendrogliomas), and necrosis and hemorrhage (generally seen in high-grade gliomas and hemorrhage also in certain metastases). Many of the same features are important in the ongoing evaluation of patients with known brain tumors. The updated version of the Response Assessment in Neuro-Oncology working group developed criteria based on MR to define response to treatment [21]. Diffusion-weighted imaging (DWI) offers insight into the diffusion of water molecules in tissues and can be used to calculate the apparent diffusion coefficient (ADC). ADC values derived from DWI have been shown to be reduced in highly cellular tumors, such as high-grade glioma. With regard to gliomas, lower ADC values have been reported in higher-grade gliomas than lower-grade gliomas, and lower ADC values have been reported to have a poorer prognosis independent of tumor grade [22].

Nuclear Imaging for Staging/Prognosis

Historical perspective. Several tracers have been used for imaging brain tumors (Table 5), and there are multiple mechanisms responsible for tracer uptake (Table 6). For several years, nuclear medicine techniques held a primary role for diagnosing brain tumors because CT entered into clinical practice in 1973 and MR a few years later. Pioneering studies with radiopharmaceuticals to detect brain tumors were carried out with ^{131}I-labeled serum albumin and, subsequently, with ^{203}Hg- or ^{197}Hg. Images were recorded with the rectilinear scanner developed by Benedict Cassen in 1950. Subsequently, with the advent of the scintillation camera (1959) [23], ^{99m}Tc-pertechnetate (^{99m}Tc), was primarily used for nuclear brain scanning. The advent of CT scanning, with markedly improved anatomic resolution, resulted in replacement of pertechnetate and ^{99m}Tc-DTPA brain scans. These radiopharmaceuticals display limited transport across the BBB in normal conditions, and the rationale to their use stemmed from altered BBB permeability in CNS pathologies. Dynamic acquisition allowed studying the perfusion of brain vessels, a procedure referred to as nuclear cerebral angiography [24].

Although thallium-201 chloride (^{201}Tl-chloride) and ^{99m}Tc-methoxyisobutylisonitrile (^{99m}Tc-sestamibi) were introduced later, both of them are no longer used today for CNS scintigraphy. ^{201}Tl ionic thallium is a substrate for the Na^+/K^+ ATPase pump, and thus ^{201}Tl uptake

Table 5 Most common current radiotracers for brain tumor imaging

Biological process	Radiotracer
Glucose transport across BBB and metabolism	[^{18}F]fluorodeoxyglucose ([^{18}F]FDG)
Amino acid transport and protein synthesis	[^{11}C]leucine
	[^{11}C]methionine ([^{11}C]MET)
	^{123}I-alpha-methyltyrosine (^{123}I-IMT)
	[^{11}C]tyrosine
	^{18}F-fluoroethyltyrosine (^{18}F-FET)
	alpha-[^{11}C]methyltryptophan
	[^{18}F]proline
Amino acid transport and dopamine metabolism	[^{18}F]fluoro-L-3,4-dihydroxyphenylalanine ([^{18}F]FDOPA)
Cellular proliferation	^{18}F-fluorothymidine (^{18}F-FLT)
	^{18}F-2-fluoro-5-methyl-1-beta-D-arabinofuranosyluracil (^{18}F-FMAU)
Somatostatin receptor imaging	^{111}In-DTPA-octreotide
	^{68}Ga-DOTANOC, ^{68}Ga-DOTATOC
Lipid metabolism	[^{11}C]choline/^{18}F-fluorocholine
Hypoxia	^{18}F-fluoromisonidazole (^{18}F-MISO)
	^{123}I-iodoazomycin arabinoside (^{123}I-IAZA)
	^{18}F-azomycin arabinoside (^{18}F-FAZA)
	^{64}Cu-methylthiosemicarbazone (^{64}Cu-ATSM)

Table 6 Factors affecting uptake of radiopharmaceuticals in gliomas

1. Perfusion and blood–brain barrier integrity
2. Histological grade
3. Glucose metabolic rate
4. DNA proliferation rate
5. Protein synthesis rate
6. Membrane (phospholipid) proliferation rate
7. Expression of membrane transporters
8. Oxygen tissue concentration (hypoxia)
9. Dimension of the lesion (partial volume effect)
10. Necrotic areas
11. Treatment with steroids
12. Radiotherapy treatment
13. Multidrug resistant phenotype
14. Expression of Na^+/K^+ ATPase
15. Expression of catecholamine binding sites
16. Glutathione content and redox potential
17. Intracytoplasmic and transmembrane esterase activity

reflects increased metabolic activity. The detection rate was reported as high as 85% [25–27], but it is important to consider that such figure was obtained with larger tumors than those investigated nowadays. False negatives were typically patients with small tumor size or tumors located in deep structures (basal ganglia and thalamus). Poor spatial resolution was the most important limiting factor for imaging. Investigators often failed to find a correlation between ^{201}Tl uptake and either tumor histology or cellular proliferation rate [28].

^{99m}Tc-sestamibi is a cationic lipophilic compound that accumulates in the cytoplasm and mitochondria as a result of passive diffusion across the negative cellular membranes. Cellular uptake is also dependent on the integrity of the mitochondrial membrane potential. Moreover, ^{99m}Tc-sestamibi kinetics is related to the multidrug resistance system (MDR1) and P-glycoprotein activity, and it may provide prognostic information about disease [29]. Thus, it was of interest to assess whether the tumor's response to chemotherapy can be predicted by ^{99m}Tc-sestamibi SPECT and whether ^{99m}Tc-sestamibi could be used for investigating the poor chemosensitivity of gliomas [30]. ^{99m}Tc-sestamibi findings were compared to the expression of the MDR1 gene and its product P-glycoprotein. SPECT in brain tumor patients showed increased uptake in patients who deteriorated clinically and negligible uptake in patients that did not recur, and MDR1 gene expression was inversely related to grade of malignancy [31]. The recent development of PET tracers for the evaluation of the MDR system drastically reduced the applications of ^{99m}Tc-sestamibi [32].

Brain Perfusion Imaging

^{99m}Tc-hexamethylpropyleneamine oxime (^{99m}Tc-HMPAO) and ^{99m}Tc-ethylcisteinate dimer (^{99m}Tc-ECD) rapidly diffuse across the BBB and distribute in the brain according to cerebral blood flow (CBF). The intracellular trapping mechanisms are different. ^{99m}Tc-HMPAO is reduced by glutathione-enriched molecules to a more hydrophilic compound that is not able to retrodiffuse. However, the redox potential of the cell also plays an important role for intracellular retention of ^{99m}Tc-HMPAO [33]. ^{99m}Tc-ECD enters the neurons and it is hydrolyzed to more hydrophilic forms by an intracellular esterase [34].

The most frequent pattern of the appearance of brain tumors is increased activity compared to the normal parenchyma [35]. Increased vascularity (i.e., blood volume) as well as increased CBF accounts for this finding. Moreover, some metabolic trapping related to glutathione activity and esterase activity has been shown for ^{99m}Tc-HMPAO and ^{99m}Tc-ECD [36]. The mean reported positive detection rate for the detection of brain tumors was around 70% with noteworthy differences among various studies attributed to the tracer (higher for ^{99m}Tc-HMPAO) and size of the lesions [35–37]. Brain tumor perfusion, measured with any of these tracers, did not correlate with tumor histology [36]. Brain tumors may also appear as a hypoactive (cold) area rather than a hot area. Cold tumors on ^{99m}Tc-HMPAO have been related to low glutathione content. Finally, heterogeneous appearance with cold areas mixed to hot areas can be found. This typically occurs in high-grade, large-sized tumors that display necrosis in their core. Similarly to other SPECT tracers, ^{99m}Tc-HMPAO and ^{99m}Tc-ECD dynamic

acquisitions and absolute measurements are not possible, and images have poorer spatial resolution than PET images. Therefore, these tracers should not be considered today of routine clinical use to study brain tumors.

2-Deoxy-2-[^{18}F]fluoro-D-glucose ([^{18}F]FDG)

[^{18}F]FDG allows measurements of tumor glucose metabolism. [^{18}F]FDG was the first PET tracer used for imaging brain tumors and it is still widely used nowadays, after more than 30 years [38]. The rationale for the use of [^{18}F]FDG is that tumor glucose consumption is increased and thus tumor metabolic activity relates to the biological behavior. Warburg first observed that, in contrast to normal differentiated cells, which rely primarily on mitochondrial oxidative phosphorylation to generate the energy needed for cellular processes, most cancer cells rely instead on anaerobic glycolysis, a phenomenon termed "the Warburg effect."

The 2-deoxyglucose (DG) model for quantifying the cerebral metabolic rate for glucose (CMR_{glc}) was defined by Sokoloff following autoradiographic experiments in rats [39]. DG is a glucose analog that differs from glucose by the substitution of fluoride atom for the hydroxyl group on the second carbon atom. It is transported across the BBB by the same transporter as that for glucose. Within the neuron, DG is phosphorylated to DG-6-P by hexokinase. Because of the lack of the hydroxyl group, [^{14}C]DG is not further metabolized and is therefore irreversibly trapped into neurons within the time frame of the experiment [39].

Patients are invited to fast for at least 6 h before tracer injection and hydrated. All modern tomographs are acquired today in 3D mode, which enable increased sensitivity and better signal-to-noise ratio. Between 125 and 250 MBq, [^{18}F]FDG is injected depending on the body weight [40]. A 10-min static acquisition is performed about 45-min postinjection (uptake period). The patient is allowed to rest in a quiet dimly lit room with eyes closed in a condition of minimal audiosensory stimulation during the uptake phase, i.e., from tracer injection to the start of PET scanning. Images are corrected for attenuation, scatter, and random coincidences. Subsequent image reconstruction is performed using filtered back projection or, more frequently, iterative reconstruction [40].

Using arterial input function, dynamic scanning, and kinetic analysis, it is possible to obtain a quantitative measurement of the parameter of interest, e.g., the cerebral metabolic rate of glucose [39, 41]. Using noninvasive approaches and a single static acquisition, it is possible to obtain qualitative or semiquantitative measurements. The standardized uptake value (SUV) and the tumor-to-non-tumor activity ratio are the most common semiquantitative indices.

According to a 2-tissue compartment, irreversible model, cerebral metabolic rate of glucose (CMR_{glc}) can be computed as follows:

$$CMR_{glc} = \frac{C_p}{LC}\frac{K_1 k_3}{k_2 + k_3} \quad (1)$$

where C_p is the mean glucose concentration, LC is the lumped constant (a factor that accounts for kinetic differences between glucose and deoxyglucose), K_1 and k_2 reflect glucose transport from plasma to brain and vice versa, and k_3 reflects glucose phosphorylation by hexokinase. The rate of DG-6-P accumulation is related to neural activity. Physiological consumption of glucose for gray matter is two- to fourfold higher than in white matter. The 2-deoxyglucose model was subsequently adapted to human studies with [^{18}F] labeling for PET.

Diagnosis and grading. Early studies in brain tumor patients stressed the importance of the functional information provided by PET compared to morphologic neuroradiological techniques. Much of this early work is credited to the group headed by Di Chiro at the National Institutes of Health [38, 42, 43]. Di Chiro et al. first used PET with [^{18}F]FDG in 23 patients with cerebral gliomas. All ten high-grade gliomas demonstrated focal tracer uptake that was easily visible (Fig. 1). Cerebral glucose utilization was often depressed in adjacent areas. Mean CMR_{glc} in high-grade gliomas was 7.4 ± 3.5 mg/100 g min. The 13 low-grade

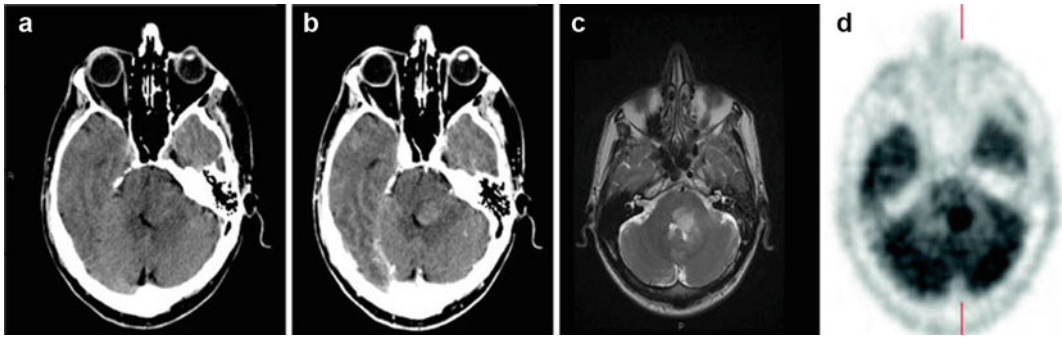

Fig. 1 A 42-year-old patient presented with headache and motor coordination impairment. Unenhanced CT (**a**), contrast enhancement CT (**b**), T2-weighted MR (**c**), and [^{18}F] FDG PET were performed. A focal area of increased glucose consumption in comparison to both *white matter* and *gray matter* is visible in the cerebellum. Visualization of the tumor is sharper on contrast enhancement CT compared to unenhanced CT. Biopsy revealed a high-grade glioma

gliomas had CMR_{glc} of 4.0 ± 1.8 mg/100 g min, with no distinctly visible hot spot. Thus, the rate of glucose metabolism was correlated to tumor malignancy [42]. This finding was considered as a major achievement because in those early times in vivo, noninvasive grading of neoplasms appeared much less intuitive as nowadays. The best cutoffs for the tumor-to-white matter ratio and the tumor-to-gray matter ratio for distinguishing high-grade gliomas and low-grade gliomas were 1.5 and 0.6, respectively. With these cutoffs, sensitivity and specificity were 94% and 77% [42]. Very similar results were obtained in a larger study 13 years later despite significant technological changes that had occurred meantime [44].

Brain tumors may induce suppression of metabolic activity in nearby normal and edematous tissue. Reduced glucose metabolism may occur also in normal brain tissue that is remote, but functionally linked to the site of the tumor (diaschisis) [45]. The cerebellum is a frequent site of metabolic reduction that is typically contralateral to the site of the tumor (crossed cerebellar diaschisis). Cerebellar hypometabolism is ascribed to functional interruption of the contralateral cerebropontine-cerebellar pathway [46].

Qualitative vs. *quantitative*. Which analysis method should be used for interpreting brain tumor images? Each analysis method has advantages and disadvantages (Table 7). PET was originally developed as a quantitative technique, and the first applications used arterial line input function for quantitative measurement of CMR_{glc}. However, for clinical purposes analysis did not always match histopathology results [47]. Moreover, a significant difference in glucose metabolism between high-grade and low-grade gliomas was not always detected [48]. This has noteworthy importance when passing from group analysis of research studies to single subject analysis of the clinical routine. Methodological considerations and technological factors cast into doubt the validity of the [^{18}F]FDG model in brain tumors. Sokoloff first noted that the lumped constant value in tumors was different from that in normal brain. Rate constants could also change as a consequence of altered metabolism [49]. Finally, tissue inhomogeneity, which is thought to introduce an overestimation of CMR_{glc} in normal cerebral tissue, is expected to have a greater effect with old scanners, because of poorer resolution [50]. By partial volume effect, measurements in a certain ROI reflect the spillover of activity into neighbor areas as well spill in of activity from neighbor areas [51]. Partial volume effect would artificially decrease CMR_{glc} in rim-shaped hypermetabolic areas for which ROI analysis would include significant amount of white matter. On the basis of these considerations, visual analysis has been advocated for clinical routine purposes, while PET quantitation with arterial line input function should be limited to restricted research protocols [52].

Table 7 Characteristics of quantitative and semiquantitative brain PET studies with [^{18}F]FDG

	Quantitative studies	Qualitative studies
Arterial input function	Necessary	Not necessary
Acquisition	Dynamic (frames ranging from 30 s to 5 min for a total of 60 min)	Static (10–15-min acquisition 45-min postinjection)
Glycemia	Necessary	Not necessary
Parameters	CMR_{glc} (mg/glc/100-g brain tissue)	SUV
		Tumor-to-non-tumor ratio
		Visual analysis
Data analysis	Time-consuming and technically challenging computer programming	None to simple (ROI analysis)
Diagnostic yield	Greater accuracy than semiquantitative analysis not proven	Sufficient for the vast majority of routine clinical tumor cases
Metabolic specificity	Not specific for tumor	Not specific for tumor
Pitfalls	Lumped constant assumed to be equal to normal brain	Visual analysis subject to subject bias
Application	Preferred for research studies	Preferred for clinical diagnostic routine

Subjectively, [^{18}F]FDG uptake within a tumor region is compared to the contralateral white matter region or, less frequently, to contralateral gray matter region. Accordingly, high-grade tumors have metabolism greater than white matter, and low-grade tumors have metabolism that is similar or lower than white matter. Semiquantitative measurements, such as SUV or tumor-to-white matter ratios, may be useful. Tumor-to-white matter ratios do not have some limits of SUV, because biases due to global factors are being canceled out as the ratio of the two ROIs is computed. Visual analysis is standard today in the clinical activity [48, 53–55].

Glucose loading. It is apparently paradoxical that, while patients are being asked to fast before a PET scan, glucose loading might have been used for increasing the diagnostic possibilities of [^{18}F]FDG PET in patients with brain tumors. Indeed, glucose loading has been used for enhancing detection of gliomas. Hyperglycemia reduces [^{18}F]FDG transport/uptake into the brain due to direct competition with the glucose transporter. This effect is less marked in brain tumors than in normal cortex because [^{18}F]FDG uptake in tumors occurs also through BBB breakdown. Thus, glucose loading resulted in an increased tumor-to-cortex ratio [56, 57]. Although this technique provided promising results and glucose loading is a relatively simple and safe procedure, this approach did not achieve widespread clinical use.

Late acquisition. Delayed or dual time point imaging is a successful approach used in oncological [^{18}F]FDG PET applications with the aim to increase sensitivity. The underlying rationale is that in many tumors, [^{18}F]FDG uptake continues beyond the usual 45-min uptake period, while at this time, the tracer has reached equilibrium between plasma and normal tissues. Because of the slower kinetic of the tracer in neoplasms compared to normal tissue, proportionally greater activity will be detected in tumor tissue compared to normal tissue as the interval from injection to imaging increases. Delayed imaging (90-min postinjection) increased the tumor-to-cortex contrast. This is due to both increased activity in the tumor as well as increased washout of the tracer from normal brain [58].

Tumor recurrence vs. *radiation necrosis*. The gold standard for distinguishing tumor recurrence from radiation necrosis is biopsy. The accuracy and specificity of biopsy can be as high as 95%, although biopsy of an edematous or gliotic site may be nondiagnostic [59]. Early studies showed that CMR_{glc} was increased in patients with tumor recurrence and low in patients with necrosis [60]. Even though these results were confirmed in study groups, false positives often occur on a patient-by-patient basis. Increased [^{18}F]FDG accumulation may occur following radiotherapy because of radiation-induced inflammation. The ratio between glucose metabolism in the tumor and in the contralateral remote white matter increases from 25% to 42% 1 day post-radiotherapy

and then decreases toward baseline values 7 days post-radiotherapy. Therefore, specificity may be as low as 40–60%, while sensitivity is generally high [61].

Stereotactic biopsy guidance. PET has the potential to increase the diagnostic yield of brain biopsy by selecting the areas that display highest tracer uptake and therefore are more likely to contain high-grade histotype. Specifically, stereotactic trajectories in areas of increased uptake are more often diagnostic and yield a higher proportion of high-grade gliomas. Based on these results, and similar findings obtained with other tracers, stereotactic PET-guided biopsy is now recommended [62].

Treatment planning. PET with [^{18}F]FDG showed promise for improving the accuracy of defining the target volume and for radiation dose escalation. An early study indicated that patients with glioblastoma multiforme can be treated with standard conformal fractionated radiotherapy if there is no [^{18}F]FDG uptake, while an additional boost is indicated in patients with increased [^{18}F]FDG uptake. [^{18}F]FDG PET volumes were predictive of survival and time to tumor progression [63]. These results, however, could not be replicated by the same group [64]. The use of [^{18}F]FDG for treatment planning remains a controversial issue considering the current more widespread use of amino acid tracers. [^{18}F]FDG might be of special interest in high-grade gliomas exhibiting marked intratumoral heterogeneity where hot spots could be possible targets for dose escalation [55].

Advantage and disadvantages of [^{18}F]FDG and of most common tracers used for brain tumor imaging are summarized in Tables 8 and 9.

Radiolabeled Amino Acids

Introduction. Neutral L-amino acids are essential amino acids; they cannot be synthesized by the brain, and, therefore, they must be supplied either by breakdown of endogenous proteins or by the diet. Since a single type of transport carrier mediates the transcapillary movement of structurally related amino acids, these compounds compete with each other for entry into the brain. After entering the neurons, amino acids may be used for protein synthesis or for other metabolic pathways.

Amino acids are the building blocks of proteins. The rate of protein synthesis is increased in proliferating brain tumors, which makes its measurement an important target for in vivo imaging. This measurement, however, held several

Table 8 Most important favorable and unfavorable characteristics of common current radiopharmaceuticals for brain tumor imaging

	Advantages	Disadvantages
[^{18}F]FDG	Easily available, overall good accuracy, good-quality images	High physiological uptake in normal brain
	Allows tumor grading	False positive by radiation necrosis and infection
	Correlates with prognosis	
Amino acid tracers	Available for PET as well as for SPECT	Tracer uptake is poorly affected by tumor grade
	Negligible uptake in normal brain	
	Optimal tumor delineation and contrast	
	Correlates with prognosis	
	Very high negative predictive value for distinguishing recurrence from necrosis	
	Useful for definition of radiotherapy plan	
^{18}F-FLT	Negligible uptake in normal brain	Uptake heavily affected by BBB integrity
	Optimal tumor delineation and contrast	Kinetic analysis with metabolite correction is required to distinguish BBB disruption from increased metabolism
	Superior to amino acid tracers for grading	
	Allows differential diagnosis between tumor recurrence and necrosis	

Table 9 Sensitivity and specificity for diagnosis of brain gliomas/gliomas recurrence for most common PET tracers[a]

Tracer	Sensitivity (95% CI)	Specificity (95% CI)	Indication	Reference	Study
[^{18}F]FDG	94%	77%	Diagnosis	[42]	Monocentric
[^{18}F]FDG	75%	81%	Necrosis versus tumor recurrence	[183]	Monocentric
[^{18}F]FDG	0.77 (0.66–0.85)	0.78 (0.54–0.91)	Necrosis versus tumor recurrence	[184]	Meta-analysis
[^{11}C]MET	0.70 (0.50–0.84)	0.93 (0.44–1.0)	Necrosis versus recurrence	[184]	Meta-analysis
[^{11}C]MET	75–95% (range)	87–100% (range)	Diagnosis	[7]	Review
^{18}F-FET	0.82 (0.74–0.88)	0.76 (0.44–0.92)	Diagnosis	[92]	Meta-analysis
^{18}F-FLT	79%	63%	Diagnosis	[185]	Monocentric

[a]Note that these values should be taken cautiously because they depend on several variables, including gold standard, clinical indication, tumor grade and dimension, sample size, analysis method, and type of study (single center, multicenter, or meta-analysis). Multitracer single studies are generally more informative for the comparison between two tracers. For these reasons, only some studies are cited

methodological restrictions. In the deoxyglucose method, intracytoplasmic trapping is the only active metabolic pathway, there are no radioactive metabolites, and computation of glucose metabolism is conceptually easy. For amino acids this is not the case. In addition to protein synthesis, amino acids can either be metabolized by transamination (rapidly followed by decarboxylation for CO_2 production) or enter other metabolic pathways. For some amino acids, typically ^{18}F-FET and ^{123}I-IMT, the intracellular metabolism is negligible and uptake is thought to reflect primarily transport across the BBB [65, 66]. Independently by the targeted biochemical process, amino acid tracers have shown to be useful for imaging brain tumors on several grounds.

[^{11}C]Methionine. Methionine (MET), an essential sulfur amino acid, is necessary for growth and development. At variance with [^{18}F]FDG, labeled amino acid uptake in normal cortex is very low. For this reason their uptake is not sensitive to visual and auditory stimulation enabling a simpler PET procedure. Most importantly, the role of amino acids in mediating an inflammatory tissue response is much less important than for glucose [67]. Thus, high specificity could be predicted. Soon after the publication of rapid high-yield procedures for labeling of methionine with ^{11}C ([^{11}C]MET), experiments were carried out to investigate the clinical role of [^{11}C]MET in various clinical settings.

Diagnostic accuracy. The overall sensitivity of [^{11}C]MET PET for distinguishing gliomas from nonmalignant lesions has been estimated to be around 75–95%, with somewhat lower values sometimes reported in low-grade gliomas, where uptake may occasionally be negligible. More interestingly, specificity of [^{11}C]MET PET ranged between 87% and 100% [68].

Grading. On the other hand, the predictive value of [^{11}C]MET PET for grading is limited. Several studies showed that [^{11}C]MET is taken up by gliomas irrespective of grade and that there is sizeable overlap in uptake values between low-grade and high-grade gliomas. Nevertheless semiquantitative analysis allows differentiating high-grade and low-grade gliomas better than visual analysis [68, 69].

Prognosis. In grades II and III gliomas, higher tumor to contralateral count ratios are associated with reduced survival. No such association was observed within the grade IV glioma group, most likely because of the overall poor prognosis in all these patients [70]. The prognostic value of [^{11}C]MET uptake has been consistently replicated in various studies [71].

Tumor extent determination. The critical factor in determining the edges of the tumors is the

method used for distinguishing significant from negligible tracer uptake. There is currently no consensus on the best method for this purpose. Visual qualitative and several semiquantitative methods have been adopted: fixed percent threshold value of tumor uptake, tumor-to-non-tumor ratios, absolute SUV values, and automatic software-based segmentation algorithm are some examples of such techniques. Irrespective of the method used, [^{11}C]MET PET delineates a larger volume in comparison to MR or [^{18}F]FDG PET. Integrating [^{11}C]MET PET with MR images is useful for planning surgery, with ensuing clinical impact in about 80% of the procedures [72–74]. The integration of [^{11}C]MET PET with morphological imaging was also useful for defining the radiotherapy plan [74, 75] (Fig. 2). PET guidance is considered necessary for defining the amount of tissue to be removed in brain tumors.

Tumor biopsy. Tumor biopsy is necessary before initiating any form of treatment. Although the poorer relation between [^{11}C]MET uptake and grading does not allow predicting the highest tumor grade, [^{11}C]MET PET has been advocated to reduce the number of required biopsy attempts and to reduce the risk of damaging functional areas in patients with brain tumors [72–74].

Therapy assessment and follow-up. Following surgical or radiation therapy, [^{11}C]MET PET can be repeated for assessing response to treatment, as well as for planning potential second-look surgeries. Prolonged survival in grades III and IV glioma patients with no [^{11}C]MET uptake after surgical resection as compared to those with residual [^{11}C]MET uptake has been reported [76].

Tumor recurrence vs. *radiation injury.* Because of limitations of [^{18}F]FDG for discriminating recurrent tumor from radiation injury, several authors investigated the usefulness of [^{11}C]MET PET (Fig. 3). Comparative evaluations show a greater accuracy of [^{11}C]MET PET than [^{18}F]FDG PET for the differential diagnosis. The use of semiquantitative binding provides a more robust tool to the differentiation of tumor recurrence from radiation injury [77].

3-^{123}I-Alpha-Methyltyrosine (^{123}I-IMT) and *O*-(2-^{18}F-Fluoroethyl)-L-Tyrosine (^{18}F-FET)

Several amino acid-derived radiopharmaceuticals can also be labeled with single-photon emitters, allowing a less expensive, more widely accessible

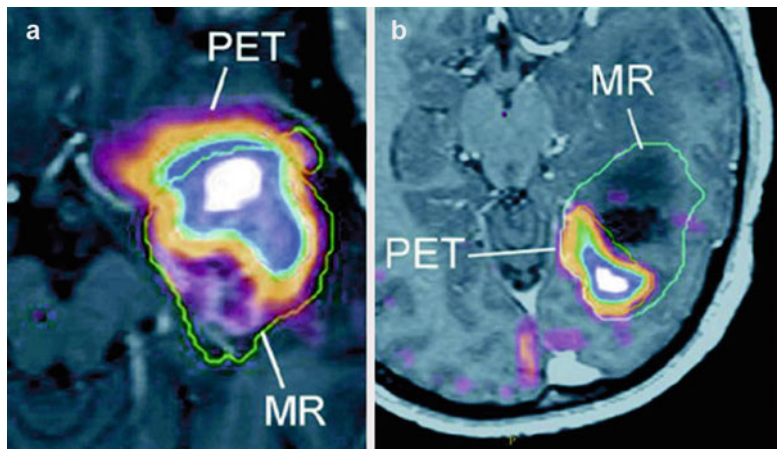

Fig. 2 Two examples of the use of PET in the definition of a radiotherapy plan. Tracer uptake on [^{11}C]MET PET is mapped with different colors according to its intensity. (**a**) Patient with left temporal anaplastic astrocytoma. PET contour projects out of the MR contour and some MR voxel extend out of the PET contour. The integration of both information will define the ultimate radiotherapy treatment plan. (**b**) Patient with left posterior temporal-occipital anaplastic oligoastrocytoma. In this case a greater discrepancy was found between the volume identified by [^{11}C]MET PET and the volume identified by MR (Reprinted with permission from Ref. [74])

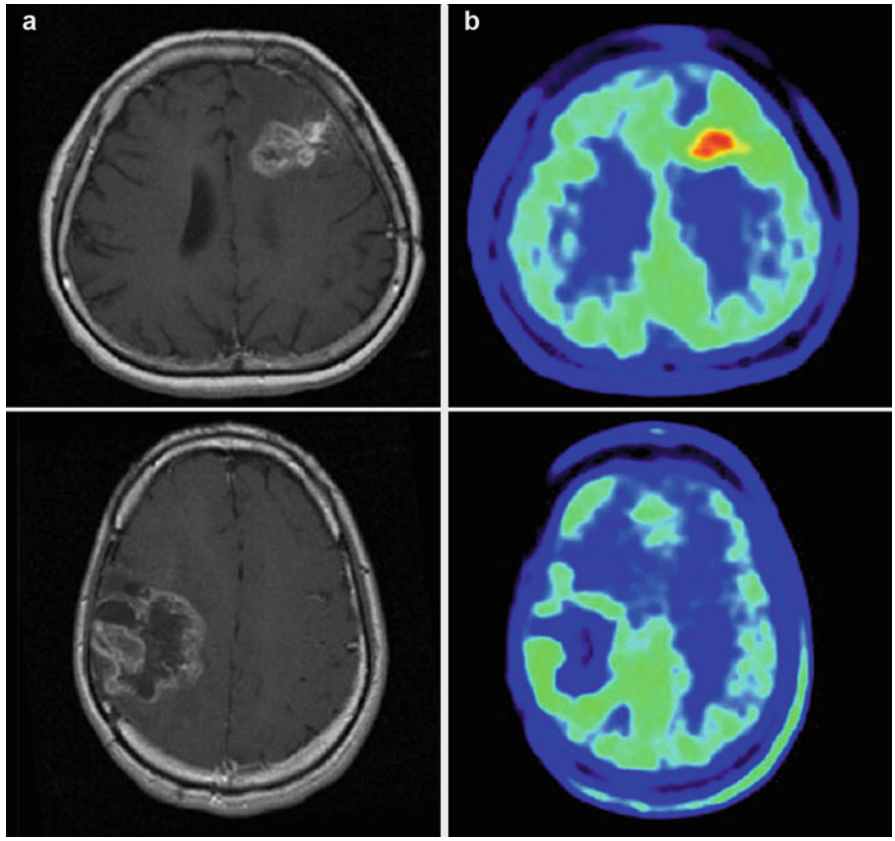

Fig. 3 (*Top*) Images of a 49-year-old woman who had been previously treated for glioblastoma multiforme with tumor resection and conventional radiotherapy at dose of 60 Gy. (**a**) T1-weighted MR image with contrast medium, obtained 13 months after initial surgery, showing contrast-enhanced lesion in the left frontal lobe. (**b**) [^{11}C]MET PET image showing focal accumulation of tracer corresponding to the abnormality on MR image. Recurrent tumor was pathologically confirmed by second surgery. (*Bottom*) Images of a 25-year-old man who had been previously treated for anaplastic astrocytoma with tumor resection and conventional radiotherapy at dose of 60 Gy. (**a**) T1-weighted MR image with contrast medium, obtained 21 months after initial surgery, showing ringlike enhancement of lesion in the right parietal cortex. (**b**) [^{11}C]MET PET image showing slight accumulation of tracer corresponding to abnormality on MR image. Gliosis without tumor was pathologically demonstrated by second surgery. Both images exemplify the primary role exerted by PET with ^{11}C-MET in distinguishing tumor recurrence from radiation necrosis (Reprinted with permission from Ref. [77])

technique for imaging protein synthesis in brain tumors. The interest has been twofold: (1) to develop and validate the clinical use of such tracers and (2) to compare the performance of SPECT tracers to PET tracers.

^{123}I-IMT may be considered the prototype of SPECT amino acid tracers. ^{123}I-IMT has a similar affinity to the neutral amino acid carrier at the BBB as L-tyrosine, but is not further metabolized and not incorporated into proteins [78]. BBB disruption and active transport through the natural amino acid carrier represent the mechanisms of tracer uptake [79]. Uptake in normal brain tissue is negligible, a feature that allows optimal contrast between tumor and surrounding normal cortex [78, 79].

The sensitivity and specificity for discriminating gliomas from nonneoplastic lesions is in about the same range as amino acid PET tracers. The accuracy is generally higher for high-grade gliomas compared to low-grade gliomas [80]. Low-grade gliomas are more difficult to

distinguish from nonneoplastic lesions owing to their lower uptake [81–83].

^{123}I-IMT SPECT has been compared to [^{18}F]FDG PET for studying tumor and non-tumor lesions. Tumor uptake ratios were higher for ^{123}I-IMT than [^{18}F]FDG. Despite the lower resolution and lower sensitivity of SPECT compared with PET, ^{123}I-IMT SPECT was superior to [^{18}F]FDG PET in the detection and delineation of tumor tissue. Better tumor delineation was obtained with PET and either [^{11}C]MET or ^{18}F-FET compared to ^{123}I-IMT SPECT [81, 84].

^{123}I-IMT SPECT may be used in radiotherapy planning. The tumor volume defined by ^{123}I-IMT uptake was compared with the volume of the hyperintensity areas of T2-weighted MR and with the volume of contrast enhancement on T1-weighted MR. ^{123}I-IMT-defined tumor volume increased the radiotherapy target volume based on T2 and T1 images by about 30–40% and led to an increase in boost volume by 20%. Current approaches recommend the use of radiolabeled amino acid SPECT or PET tracers for definition of the target volumes for radiotherapy planning [85].

The wider availability of PET/CT scanners led to an increase of the use of ^{18}F-FET [86]. After i.v. administration ^{18}F-FET is taken up by both tumor and normal brain tissue. ^{18}F-FET uptake increases in normal gray and white matter to reach a plateau 20-min postinjection and the value remains stable until 120-min postinjection [87, 88]. In brain tumors, ^{18}F-FET kinetics depends on histology and grade. ^{18}F-FET is taken up by neoplastic cells, but is not incorporated into proteins, in contrast to natural amino acids such as [^{11}C]MET, which has a 15% incorporation rate [89, 90]. The uptake mechanism of ^{18}F-FET tracer is complex and not fully understood, but it seems to involve multiple pathways, including the specific LAT1 subtype system and the ubiquitous Na-dependent system $B^{0,+}$ and B^0 [91, 92].

As to the imaging protocol, patients should be fasting for about 4 h before trace injection to avoid saturation with unlabeled L-amino acid modifying FET transport into tumor cells. After injection, PET images are dynamically acquired for about 40–60 min (8–12, 5-min frames, or 4–6, 10-min frames) [86, 93].

^{18}F-FET PET image analysis provides both qualitative and quantitative information. The use of last acquired averaged frames (40–50 or 50–60 min) allows the reduction of brain–blood noise and improves the signal-to-noise ratio. Lesion maximum and SUV_{mean} are usually determined by averaging later frames. Moreover, using a manually drawn or an automatic region of interest (ROI), the contralateral normal brain uptake and maximum and mean tumor-to-background ratios (TBR_{max}, TBR_{mean}) may be computed. By locating ROIs on all slices in which the tumor is represented, a volume of interest (VOI) around the tumor is generated, on each frame of the dynamic acquisition to compute time–activity curves [12],

Numerous, but usually small studies assessed ^{18}F-FET PET value in the diagnosis of primary brain tumors. ^{18}F-FET PET was shown to be more accurate than ^{123}I-IMT SPECT [84], [^{18}F]FDG [12, 94], ^{18}F-fluorothymidine PET [95], and ^{18}F-fluorocholine PET [96] to detect brain tumors.

A recent meta-analysis of 13 studies on the use of ^{18}F-FET PET in primary brain tumor including 462 patients showed sensitivity and specificity of 82% (95% confidence interval 74–88%) and 76% (44–92%), respectively [92]. Using ROC analysis TBR_{mean} and TBR_{max} higher than 1.6 and 2.1, respectively, provided the best diagnostic value for differentiating primary brain tumors from non-tumoral lesion. Moreover, TBR_{mean} and TBR_{max} were significantly lower in grade I–II gliomas as compared with grade III–IV gliomas.

Even though on a group basis, SUV and TBR allow identification of differences in ^{18}F-FET uptake and metabolism between gliomas and non-tumoral lesions, on a single subject basis, this discrimination is more difficult because of metabolic overlap found among the different WHO grades [92]. Analysis of time–activity curves allows improving the differentiation between low- and high-grade gliomas. Early (<15 min) maximal uptake followed by a decreasing curve has been related to high-grade glioma, and late (>15 min) maximal uptake followed by a steadily rising curve has been related to low-grade tumor [97–99].

L-3,4-dihydroxyphenylalanine ([^{18}F]fluorodopa, [^{18}F]FDOPA). Among other amino acid

tracers, a growing important role is being played by [^{18}F]FDOPA, which is also sensitive to dopamine metabolism. Other than in the striatum and the substantia nigra, where the uptake of the tracer is physiologically high, [^{18}F]FDOPA displays low uptake in all the remaining brain areas. Contrary to studies performed for the diagnosis of movement disorders, where a dynamic scan or a late scan acquisition at about 70 min are performed, for tumor imaging, an early scan at 20-min post-injection is preferred. With ongoing interval from injection, the specific uptake in the striatum increases, and it may mask either the visualization or tumor in the proximity of the basal ganglia or other tumors that have low [^{18}F]FDOPA uptake. At 20-min p.i., the uptake in tumor is on the contrary similar or higher than in the basal ganglia [100].

[^{18}F]FDOPA PET/CT is highly sensitive and specific for the detection of glioma recurrence, it is superior to [^{18}F]FDG, and it is especially advantageous in patients with low-grade gliomas [101, 102]. Tripathi et al. directly compared the performance of [^{18}F]FDOPA, [^{18}F]FDG, and ^{18}F-FLT in evaluating primary and recurrent low-grade gliomas. SUV_{max} for [^{18}F]FDOPA was two to three times higher than for ^{18}F-FLT, but it was lower than and for [^{18}F]FDG. This shows that ^{18}F-FLT uptake is generally low in gliomas. The authors concluded that [^{18}F]FDOPA is superior to ^{18}F-FLT and [^{18}F]FDG for low-grade gliomas [103].

It was also shown that PET/CT with [^{18}F]FDOPA has greater diagnostic power compared to MR for the differential diagnosis between tumor recurrence and radiation necrosis. Specifically, sensitivity, and accuracy were 92.3%, 44.4%, and 80% for MR and 100%, 88.9%, and 97.1% for [^{18}F]FDOPA [102].

A very interesting study [100] was performed to address the comparative value of [^{18}F]FDOPA versus [^{11}C]MET, which is the most widely used amino acid tracer for detecting tumor recurrence and generally considered as the gold standard. [^{11}C]MET and [^{18}F]FDOPA images matched in all patients and showed all lesions as hot spots with higher uptake than in the contralateral brain. SUVs and tumor/contralateral did not statistically differ between the two tracers. The authors concluded that [^{18}F]FDOPA is accurate as a surrogate for [^{11}C]MET in imaging amino acid transport in malignant cerebral lesions for the purpose of visualization of vital tumor tissue. It combines the good physical properties of ^{18}F with the pharmacological properties of [^{11}C]MET and might therefore be a valuable PET radiopharmaceutical that can be more widely used for brain tumor imaging in centers without a cyclotron [100].

Tumor proliferation. Increased cell proliferation rate is a well-known hallmark of cancer. The key step for cell proliferation is DNA synthesis. Thus, different radiotracers were developed to assess in vivo DNA synthesis. Thymidine is a pyrimidine used for DNA but not for RNA synthesis. This selectivity made this compound the first choice for assessing proliferation. Thymidine is incorporated into DNA through the exogenous (salvage) pathway for pyrimidines, through phosphorylation to thymidine triphosphate. The salvage pathway represents only a minor source for thymidine synthesis because the majority of thymidine is synthesized through the de novo pathway. Nevertheless, as the two pathways are competitive in physiological conditions, both are informative on DNA synthesis, while only the salvage pathway can be measured for the limited number of compartments involved and modeling assumptions. Imaging of DNA proliferation was expected to be superior to imaging of glucose metabolism for assessing response treatment, because cells may maintain their oxidative and glycolytic function in spite of impaired DNA synthesis [104].

Initial PET studies were performed with [^{11}C]thymidine. This tracer is rapidly metabolized producing several labeled compounds, primarily [^{11}C]CO_2, that retrodiffuses into the brain affecting the time–activity curve [105]. The exponentially growing complexity of metabolites correction combined to the low signal-to-noise ratio due to ^{11}C-labeling limited the use of this compound.

More recently, 3-deoxy-3-^{18}F-fluorothymidine (^{18}F-FLT, a thymidine analog) was developed. ^{18}F-FLT offers the advantages of ^{18}F-labeling and a more favorable radiometabolite profile [106]. However, the blood–brain barrier limits cellular uptake of ^{18}F-FLT [107]. ^{18}F-FLT uptake is a function of the plasma input function and the rate of its

transport across the blood–brain barrier; therefore, a complete kinetic model of ^{18}F-FLT uptake, transport, and metabolism is needed to accurately quantify DNA synthesis in brain tumors [108]. Without such a model, ^{18}F-FLT is unlikely to perform better than an inert contrast agent, such as gadolinium chelates, in brain tumor imaging. The assumption that ^{18}F-FLT standardized uptake value reflects primarily the uptake of the tracer into the DNA synthesis pathway is potentially misleading in CNS neoplasms [109].

Patients with brain tumors have increased tracer incorporation (K_i). In high-grade tumors where CBF is also increased, the increased tracer incorporation may partially be related to blood flow [107] (Fig. 4).

Probably owing to the difficult modeling strategy, findings differed among studies. For example, authors reported a significant correlation between ^{18}F-FLT K_i or k_3 and Ki-67 immunostaining, while no significant correlation was found for ^{18}F-FLT uptake ratios [108]. Others reported that uptake ratios have similar power as kinetic analysis to predict long-term survival [110]. ^{18}F-FLT (83%) had slightly lower sensitivity than [^{11}C]MET (88%), and both tracers have 100% specificity. SUV_{max} for [^{11}C]MET was significantly higher in high-grade gliomas compared to low grade, although there was a wide overlap. For ^{18}F-FLT, the difference was more relevant. ^{18}F-FLT was slightly superior to [^{11}C]MET for tumor grading. Although the two tracers explore two different biological processes, there is no substantial additional advantage by their sequential use [111].

Radiolabeled choline. Radiolabeled choline (either [^{11}C]choline or ^{18}F-fluorocholine), a phospholipid precursor, is a tumor-seeking radiopharmaceutical that has emerged because of its alleged potential to image membrane proliferation. While it is known that choline is a precursor of phospholipids (through the synthesis of phosphorylcholine), there are currently insufficient data to support the assumption that [^{11}C]choline labels uniquely membrane phospholipids. The rationale behind the clinical use of this PET tracer derived from in vivo studies with proton magnetic resonance spectroscopy showing elevated signal of choline-containing compounds (i.e., phosphorylcholine and glycerophosphocholine) in brain tumors [69]. Other metabolic pathways include the synthesis of acetylcholine and conversion to

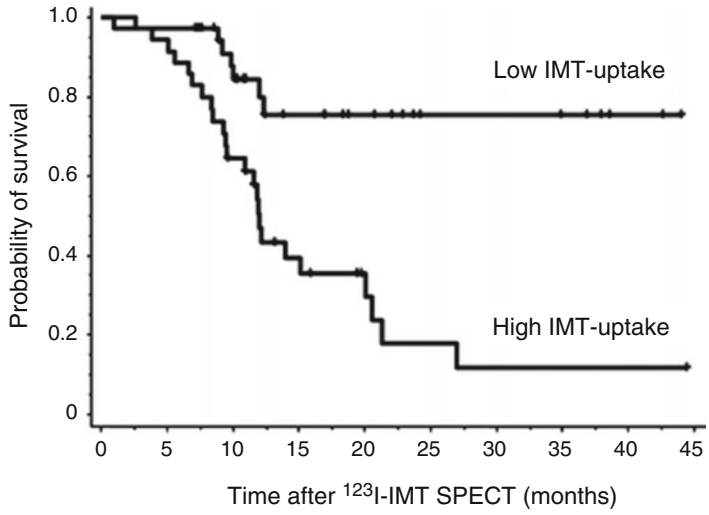

Fig. 4 Kaplan–Meier curves of overall survival among patients with postoperative low ^{123}I-IMT uptake and high ^{123}I-IMT uptake. Survival is significantly shorter in patients with ^{123}I-IMT uptake ratio >1.7 compared to patients with ^{123}I-IMT uptake ratio <1.7. The figure exemplifies the high prognostic power of functional nuclear medicine techniques, even in the case of SPECT (Reprinted with permission from Ref. [83])

betaine, while a significant amount of precursor remains unmetabolized in the cytoplasm [69]. However, regardless of the measured biochemical process, [^{11}C]choline did show to be useful for imaging and for assessing the response to therapy of gliomas and meningiomas.

The tracer displayed an excellent capability to delineate the tumor contours due to the negligible uptake by normal brain. As already noted for PET with amino acid tracers, this feature has been shown to be useful to guide biopsy and for radiotherapy planning [112]. Nevertheless, pitfalls may also occur. False positives are generally of greater concern than false negatives and are due to some accumulation of the tracer in inflammatory lesions [113]. Increased tracer uptake may occur also in brain metastases from other tumors and in meningiomas [114].

Higher [^{11}C]choline uptake has been reported in high-grade gliomas compared to low-grade gliomas [115]. Presently, there are discrepant findings on the issue whether [^{11}C]choline tumor metabolism, as measured by PET/CT, predicts [115–117] or does not predict tumor grade [69]. In a multitracer study, tracer uptake was significantly higher in high-grade gliomas than in low-grade gliomas for [^{11}C]choline, but not for [^{18}F]FDG [116]. However, [^{11}C]choline PET/CT could not differentiate between low-grade gliomas and benign lesions because of the relatively low uptake in low-grade tumors [116]. In a large study enrolling 94 patients with suspected brain tumor, [^{11}C]choline had greater accuracy than [^{18}F]FDG (84% vs. 71%). The authors concluded that, after accounting physiological variants and potential pitfalls of the tracer, [^{11}C]choline might have greater potential than [^{18}F]FDG for brain tumor PET imaging [113]. Another multitracer study compared [^{11}C]MET, [^{11}C]choline, and [^{18}F]FDG. The authors measured the ratio of tumor uptake to normal brain uptake (T/N ratio), using the frontal cortex as reference region, and analyzed the correlations between tracer uptake and tumor grade, type, and proliferation activity. Whereas all three tracers showed a similar correlation between the T/N ratio and tumor grade in astrocytic and oligodendroglial tumors, [^{11}C]MET enabled the most straightforward visual localization of hot lesions [118].

Until now, there have been few applications of [^{11}C]choline PET/CT for radiation therapy planning. [^{11}C]choline PET/CT could better delineate the boundaries between lesions and surrounding normal brain tissues compared with MR, and the standard radiotherapy target volume was changed in 31% of patients [117]. In posttreatment patients with high-grade gliomas, lower [^{11}C]choline uptake predicted longer survival [119]. [^{11}C]choline PET/CT can be used to distinguish brain tumor recurrence from necrosis after radiotherapy with sensitivities and specificity that might be higher than those of MR [120].

Imaging tumor hypoxia. Hypoxia is defined as reduced O_2 tissue concentration. Hypoxia in tumors is associated with progression, as well as resistance to radiotherapy and to some chemotherapy regimens. Several bioreductive radiopharmaceuticals have been evaluated as hypoxia tracers. These tracers include nitroimidazole compounds, e.g., ^{18}F-fluoromisonidazole (^{18}F-MISO), ^{123}I-iodoazomycin arabinoside (^{123}I-IAZA), ^{18}F-azomycin arabinoside (^{18}F-FAZA), and ^{64}Cu-labeled methylthiosemicarbazone (^{64}Cu-ATSM). The common feature of these different tracers is that tissue binding is sensitive to tissue oxygen concentration. Specifically, as the tissue oxygen level decreases, irreversible trapping increases. Different parameters are being used to quantify tissue binding, including tissue-to-plasma ratios, SUV_{max}, a percent threshold of SUV_{max} (hypoxic volume), distribution volume (derived from the plasma input function), and pixel-based maximum-intensity-projection plots obtained using statistical parametric mapping. The correlation of such parameters with tissue oxygen tension measured with fine needle oxygen electrodes (the gold standard for measuring hypoxia) is generally not performed in humans because such procedure is invasive [121].

PET studies of brain tumor hypoxia are relatively scant and mostly limited to the use of ^{18}F-MISO [122]. ^{18}F-MISO freely crosses the blood–brain barrier and rapidly equilibrates within tissues independently of perfusion [123]. Tracer uptake in glioblastomas multiforme is heterogeneous. Increased ^{18}F-MISO tumor uptake is generally found in the periphery but not in the

center of glioblastomas multiforme (Fig. 5). The latter finding is expected, because only viable cells are able to accumulate ^{18}F-MISO, and delivery to necrotic tissue is low. This pattern is also consistent with the spatial distribution of the hypoxia-inducible factor 1 that is more expressed in tumor areas adjacent to necrosis but not in necrosis per se [124].

No correlation was found between delayed ^{18}F-MISO uptake and [^{15}O]water distribution in brain tumors, thus indicating that hypoxia may occur also in cerebral areas with normal CBF. Hypoxic volume measured with ^{18}F-MISO is a significant prognostic factor for survival. ^{18}F-MISO uptake was greater in high-grade gliomas than in low-grade gliomas [125]. In a more recent prospective study of glioma patients who underwent both ^{18}F-MISO and [^{18}F]FDG PET examinations, ^{18}F-MISO PET showed an improved ability to distinguish glioblastoma from lower grades as compared to [^{18}F]FDG [126].

PET/MR

The development of magnetic field-insensitive PET detector technology paved the way from PET/CT to hybrid PET/MR systems, which have been commercially available since 2011. Due to the higher contrast between gray and white matter, MR provides a substantial advantage over CT for diagnosing CNS lesions [127]. For scanning neurological patients, the combination of both PET and MR has often proven to be superior to the single modality approach, with improved workflow and an increase in patient comfort. The ability to characterize different pathophysiological diseases features can be useful especially in research [128]. The acquisition of MR also allows correction for partial volume effect. PET or PET/CT studies vs. MR had shown that, irrespective of the tracer, PET provides more accurate information. PET/MR studies with dedicated PET/MR scanners are now similarly providing evidence of the additional information and synergistic effect of these two techniques.

Studies with PET/MR scanners in brain tumor patients have been so far limited; therefore, we will report about studies that compared PET to MR as well as studies that used dedicated PET/MR hybrid systems.

One study reported a greater accuracy of [^{18}F]FDG PET in comparison to MR for the prediction of survival in patients with high-grade glioma after therapy with temozolomide [129].

Ohtani et al. compared [^{11}C]choline PET, contrast-enhanced MR imaging, and [^{18}F]FDG PET in 22 patients with suspected brain tumors. They found a correlation between [^{11}C]choline and the histological tumor grade, with higher uptake in high-grade gliomas. The authors suggested that the combination of [^{11}C]choline PET and MR imaging could improve the detection of high-grade gliomas. However, [^{11}C]choline PET could not differentiate between low-grade gliomas and benign lesions [116].

Tan et al. used [^{18}F]FDG, [^{11}C]choline PET/CT, and MR to differentiate brain tumor recurrence from necrosis after radiotherapy in 55 patients. Sensitivities of MR, [^{18}F]FDG, and [^{11}C]choline PET/CT in lesion diagnosis were 87%, 77%, and 92%, respectively, and their specificities were 81%, 63%, and 88%, respectively. These results suggested that [^{11}C]choline PET/CT, having higher sensitivity and specificity, may perform better in distinguishing recurrent brain tumor from radionecrosis compared with [^{18}F]FDG PET/CT and MR [120].

Boss et al. reported that the MR and PET data acquired in ten patients was of high diagnostic quality and that there was a high level of concordance between tumor-to-background ratios derived from PET/CT and those derived subsequently from PET/MR [130]. The same group later used MR spectroscopy and [^{11}C]MET PET to classify inconclusive MR findings as either low-grade gliomas or high-grade gliomas and to identify the most malignant parts within tumors before surgery. They found that areas with maximum [^{11}C]MET uptake provided satisfactory tumor grading. The spatial overlap between cerebral areas of high PET uptake and highest metabolite concentrations determined by MR spectroscopy was limited, which suggests that the diagnostic gain provided by MR

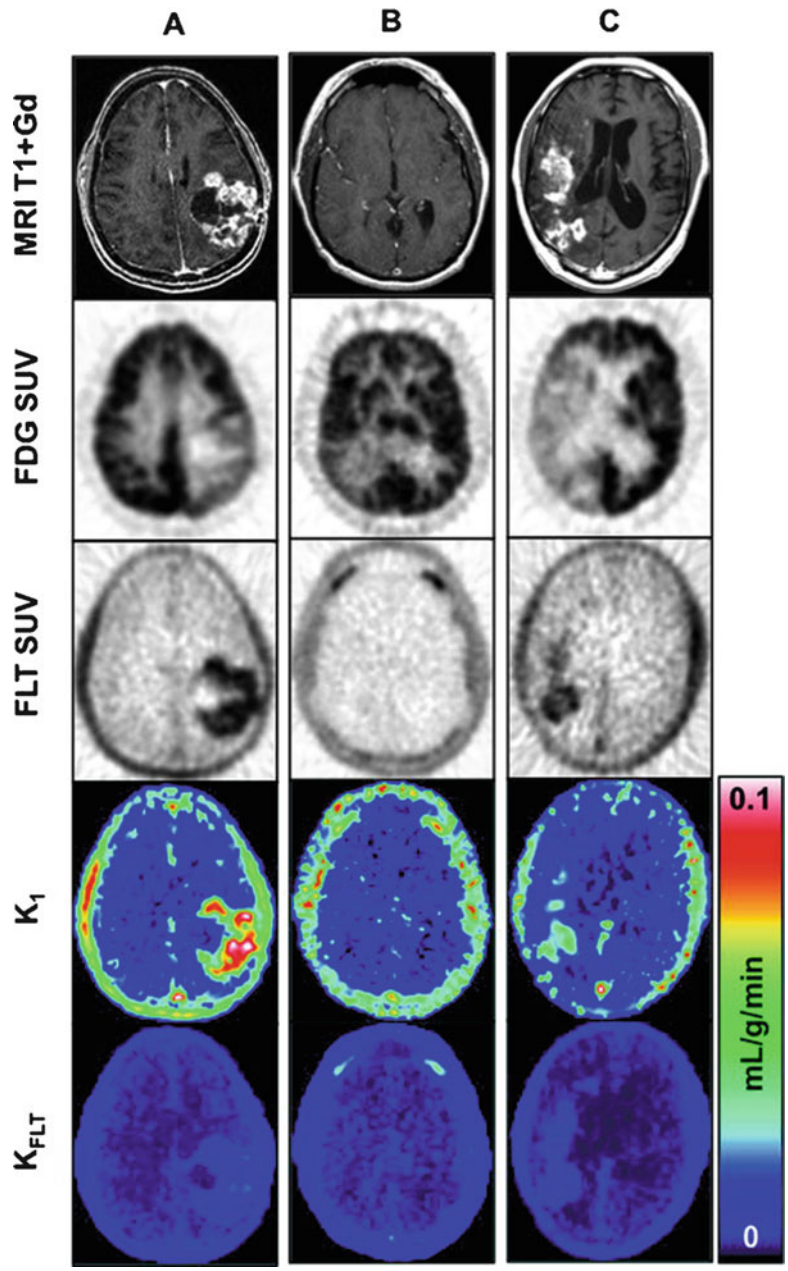

Fig. 5 Three scenarios with different aspects of ^{18}F-FLT and [^{18}F]FDG metabolism are presented. (**a**) A 44-year-old woman with recurrent grade III anaplastic astrocytoma of the left parietal cortex with BBB breakdown treated previously by radiotherapy (59 Gy). (**b**) A 56-year-old man with right parietal grade II oligodendroglioma with intact BBB treated previously by surgical resection followed by chemotherapy. (**c**) A 46-year-old man with recurrent grade II oligodendroglioma of the left temporal and parietal cortex with BBB breakdown treated with radiotherapy (54 Gy) and temozolomide before PET. Surgery and therapy occurred at least 2 years before PET for all three patients. Coregistered images are as follows: MR T1-contrast enhancement; [^{18}F]FDG SUV summed 30–60 min; ^{18}F-FLT SUV summed 30–60 min; parametric map of transport, K_1; and parametric image of metabolic flux, K ^{18}F-FLT. This figure exemplifies two different concepts: (1) the different patterns of various tracers in the same tumor depend on tumor metabolism and BBB integrity; (2) it shows how [^{18}F]FDG uptake is less influenced by BBB breakdown (it is reduced in (**a**) and (**c**) where BBB is disrupted), while ^{18}F-FLT uptake increases notably with BBB disruption (**a** and **c**), but ^{18}F-FLT does not enter the brain if BBB is normal (**b**) (Reprinted with permission from Ref. [107])

spectroscopy is limited [131]. A whole-body hybrid PET/MR system was used in another study by Preuss et al. to obtain [^{11}C]MET PET and MR imaging data necessary for biopsy planning and neuronavigation in a small series of pediatric patients with brain tumor. Representative histopathological specimens were obtained in all patients. Additional anesthesia as well as CT-related radiation exposure could also be avoided [132]. In another small PET/MR series mainly in patients with high-grade gliomas, both modalities provided sufficient diagnostic quality, and the ^{18}F-FET PET findings were in accordance with those of conventional MR [133]. All combined PET/MR imaging studies discussed above agree on the convenience of obtaining all necessary imaging parameters in one session with excellent spatial coregistration of MR and PET data. Moreover, Dunet et al. demonstrated the superiority of the combination of dynamic ^{18}F-FET PET and diffusion-weighted MR over the single modality approach for glioma grading and argued in favor of combined ^{18}F-FET PET/MR in the initial assessment of primary brain tumors [134]. They reported that tumor time–activity curve reached the best accuracy (67%) when considered alone to distinguish between low- and high-grade gliomas, followed closely by ADC histogram analysis (65%). The combination of time–activity curve and apparent diffusion coefficient (ADC) histogram analysis improved the sensitivity to 86% and the specificity to 100% [134].

Assessing the Efficacy of Treatment

The diagnostic value of MR and CT concerning changes in tumor size or contrast enhancement in response to therapy is limited because the known reactive transient BBB alterations with consequent contrast enhancement may mimic tumor progression. This phenomenon, the so-called pseudoprogression, is seen in 20–50% of cases and can lead to unnecessary overtreatment [135]. For this reason, the use of PET appears today as an ideal tool; in fact the efficacy of therapy has been assessed with different radiotracers across times.

Several studies indicate that glucose metabolism, at initial presentation, at recurrence, or in response to therapy, is predictive of survival.

In case of recurrent tumor, the mean survival time of patients with gliomas exhibiting high glucose utilization was shorter than in patients with low glucose utilization (5 vs. 19 months) [136]. Similar results were obtained by Alavi in a study that included mostly treated patients [137]. He reported estimated median survival of 33 months for hypometabolic lesions and 7 months for hypermetabolic lesions. Furthermore, in the subgroup of high-grade gliomas, it was possible to divide patients into a group with low and a group with high metabolic activity with 1-year survival rates of 78% and 29%, respectively [137]. In the setting of recurrence, these results were confirmed by Santra et al. [138]. In a more recent study, Colavolpe et al. retrospectively assessed pretreatment PET scans qualitatively and quantitatively in 41 patients with high-grade gliomas [139, 140]. The authors performed multivariate analysis including traditional prognostic factors (age, KPS, extent of surgery, and histological grade) in addition to either visual metabolic grade or the ratio between the tumor and contralateral SUV_{max}. The semiquantitative evaluation in the pretreatment of [^{18}F]FDG PET/CT provided significant additional prognostic information in newly diagnosed high-grade tumors, it was statistically more robust than the visual evaluation, and it was independent of traditional prognostic factors [139].

PET has been shown to be useful for monitoring the response to chemotherapy. Following treatment with temozolomide, the percentage of decline of CMR_{glc} versus baseline is greater in clinical responders than in nonresponders [141]. In another study, it was shown that early changes in glucose metabolism predicted response to temozolomide, but not temozolomide plus radiotherapy. In the first scenario, a greater metabolic reduction after therapy predicts longer survival [129]. One study reported the greater accuracy of [^{18}F]FDG PET in comparison to MR for predicting survival after therapy [129]. A recent publication based on the National Oncologic PET Registry examined retrospectively data from 479 patients with primary

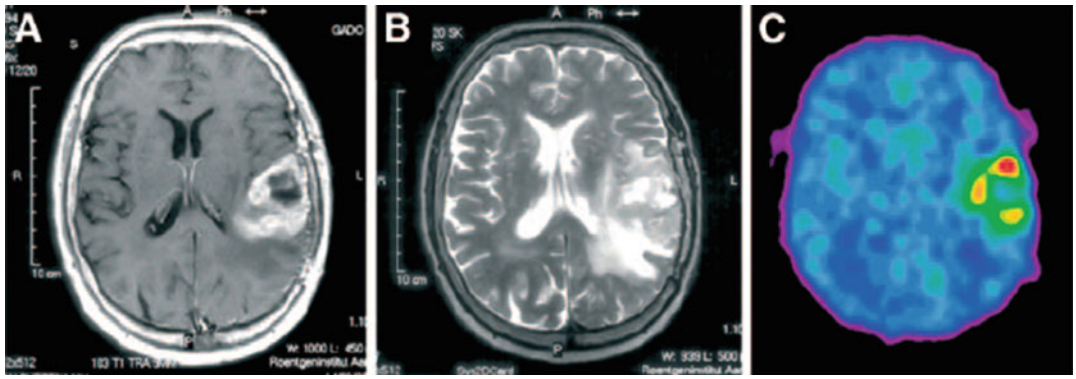

Fig. 6 Gadolinium contrast-enhanced T1- (**a**) and T2-weighted (**b**) MR images in a patient with glioblastoma multiforme in the left temporal lobe. (**c**) Late PET images show ^{18}F-MISO tumor uptake 150–170 min after injection. The figures typically identifies the behavior of a hypoxia tracer that accumulates less in the center of a lesion, where the tissue is hypoxic, and highly accumulates in the periphery of the lesion, where the tumor tissue is well oxygenated (Reprinted with permission from Ref. [124])

brain tumors (72%) or brain metastasis (28%) and found that overall, [^{18}F]FDG PET imaging changed the intended management in 38% of patients with primary brain tumors [142].

^{123}I-IMT uptake has prognostic implications. In patients who had undergone tumor resection 4–6 weeks before SPECT imaging, significant ^{123}I-IMT uptake after tumor resection was associated with shorter survival (Figs. 6 and 7). ^{123}I-IMT uptake ratio remains a significant prognostic factor when age and grading are included in a multivariate model [83].

^{18}F-FET imaging was also shown to have prognostic implications. In low-grade gliomas, baseline low ^{18}F-FET uptake predicted longer time to progression and time to malignant transformation; high uptake predicted conversion into a high-grade glioma [143]. ^{18}F-FET can be used to quantify residual tumor volume after surgery and postsurgical tumor volumes evaluated by PET predict progression-free and overall survivals [144]. Finally, patients with higher decrease in ^{18}F-FET uptake after antiangiogenic therapy with irinotecan–bevacizumab displayed longer survival [145]. Galldiks et al. compared changes in ^{18}F-FET TBR_{max} and TBR_{mean} as well as gadolinium contrast enhancement in 25 glioblastoma patients who underwent radiochemotherapy with temozolomide. Changes in TBR_{max} and TBR_{mean} between therapy and baseline predicted overall survival and progression-free survival, while gadolinium-volume changes did not [146].

Harris et al. created parametric response maps of ^{18}F-FLT and [^{18}F]FDOPA before and at two time points after bevacizumab treatment. They reported that an increase in [^{18}F]FDOPA or ^{18}F-FLT uptake on parametric response maps after bevacizumab treatment predicted shorter progression-free survival and that [^{18}F]FDOPA additionally predicted overall survival in recurrent gliomas [147].

[^{18}F]FDOPA was used at baseline, 2 and 6 weeks after the start of bevacizumab therapy for assessing response to therapy. [^{18}F]FDOPA metabolic tumor volume, but not SUV, predicted overall survival and progression-free survival. Interestingly, absolute metabolic tumor volume at 2 weeks after therapy was the strongest predictor of survival [148].

Additional Value of SPECT/CT and PET/CT vs Stand-Alone SPECT and PET

Radionuclide imaging has per se the capability of identifying disease at early stages, since it visualizes molecular targets that may change before structural tissue changes occur. Adding the CT component may improve correction for photon attenuation, but also allows for easier correlation of areas with

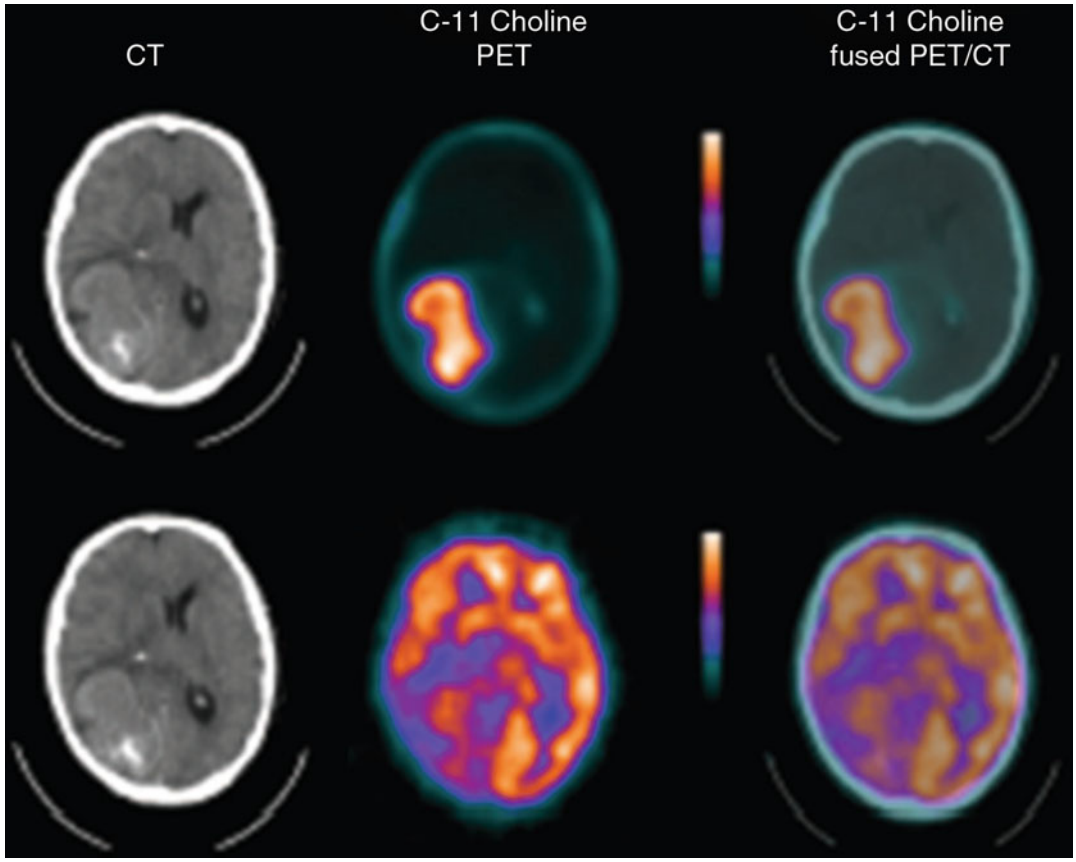

Fig. 7 CT, PET, and fused PET/CT images of a WHO grade II meningioma. CT shows a meningioma in the left temporo-occipital region that reaches medially the ipsilateral thalamus and striatum. There is high [^{11}C]choline uptake in the tumor (*top*), as well as heterogeneous increase in [^{18}F]FDG uptake (*bottom*). Note, however, the different location of the areas of increased [^{11}C]choline uptake (maximal in the posterolateral part of the tumor) and [^{18}F]FDG uptake (maximal in the anteromedial part of the tumor) (Reprinted with permission from Ref. [186])

physiological variants or abnormal tracer accumulation to anatomical landmarks [149].

So far, data on the added value of combined SPECT/CT and PET/CT examinations of the brain remain scanty. In principle, the diagnostic value of various cerebral SPECT examinations, such as cerebral perfusion or receptor studies, might be increased, to some extent, by additional CT examinations. However, considering that the morphological gold standard is represented by MR, the impact of the additional CT component on the diagnosis and clinical management of the patient is actually quite limited.

Low-dose CT is associated with relatively low radiation doses of 1–4 mSv and should be sufficient for anatomic referencing of SPECT lesions and attenuation correction. In clinical practice, if a recent enhanced CT scan is available, then another contrast-enhanced CT scan will not be repeated during SPECT/CT. For this reason, the use of low-dose, nonenhanced spiral CT is generally recommended when SPECT/CT is performed for anatomic referencing or attenuation correction [150]. This holds true also for brain tumor patients since virtually all patients referred to SPECT/CT or PET/CT will have already performed a diagnostic CT or MR. Low-dose CTs are generally acquired with a tube current of 20–40 mA and tube voltage of about 120–140 kV [150].

Usually, CT scan-based attenuation correction of brain SPECT data may lead to improved image quality and more accurate evaluation. In fact, it was shown that attenuation correction based on individual CT scans produces more accurate results than traditional methods based on the uniform linear attenuation coefficient [151].

Some studies have demonstrated the usefulness of SPECT/CT for accurate preoperative detection and localization, for radiotherapy planning, and for treatment monitoring of brain tumors [149]. SPECT/CT achieves precise anatomical localization of viable tumor lesions versus adjacent sites with physiological tracer uptake, such as the ventricles, choroid plexus, and venous sinuses [152, 153], with a proven clinical impact on management in 43% of patients [152].

Common Therapies

Primary brain tumors have a dismal prognosis. Five-year survival rates can be as low as <5% for glioblastoma, 30% for astrocytomas, but up to 100% for benign neoplasms as meningiomas. These rates have remained virtually unchanged over the last years, thus indicating the lack of substantial improvement in prognosis in spite of technological advances in diagnostic and surgical strategies [8].

Therapy is generally a combination of surgery, chemotherapy, and radiotherapy or radioimmunotherapy. Because of the limited efficacy and potentially severe side effects of each treatment, many studies are in progress to enhance the efficacy of this multimodality approach.

Surgery. Surgery remains the primary therapeutic approach for most brain tumors. The goal of surgery is twofold. First, it is necessary for definitive histological diagnosis of the tumor. Second, it allows tumor debulking, which is necessary for preventing or alleviating symptoms. Based on the extent, resections can be classified as either partial or complete. However, except for pilocytic astrocytomas, the necessary extent of surgical resection beyond obtaining a tissue for diagnosis remains controversial. Partial resections are performed for large, deeply infiltrating neoplasms for which only debulking is possible or for neoplasms located near difficult-to-access regions. Complete resection is otherwise preferred. Even normal astrocytes and oligodendrocytes can move preferentially along the preformed fiber paths in the brain, and neoplastic cells often exhibit that capacity even more. Even complete solid tumor removal (or any other local therapy) will not reach these cells, and they will likely cause tumor recurrences. Although a larger resection has greater curative potentials, the surgeon always faces a balanced compromise between the likelihood of increasing the local control and the risk of causing important side effects [4, 109].

Radiation therapy. Radiation therapy has been used extensively in the treatment of malignant and aggressive intracranial tumors, and its use has been associated with prolonged disease-free survival, but not with overall survival [4, 154]. Because of potential side effects, radiation therapy is often deferred until there are signs of progressive recurrence or malignant transformation [4, 154]. In the case of GBM, radiotherapy is complicated by the diffuse infiltrative nature of the disease and by its extreme radioresistance. However, a clear gain of median progression-free survival of GBM patients was also reported [4, 154].

Chemotherapy. The overall efficacy of chemotherapy in brain tumors is limited because the BBB limits access to the brain for molecules with low molecular weight and high lipophilicity, and the multidrug resistance system limits the efficacy of a wide range of drugs. Temozolomide is now the most effective drug and it is approved for refractory anaplastic astrocytoma or GBM [155]. The combination of radiotherapy, lomustine and temozolomide, yielded promising long-term survival data in patients with newly diagnosed glioblastoma, albeit with greater acute toxicity [156, 157].

Antiangiogenic therapy. Neoangiogenesis is another potential target for therapy of gliomas. High-grade gliomas demonstrate high levels of angiogenesis. Antiangiogenic drugs were developed to target vascular endothelial growth factor (VEGF) and VEGF receptor. Emerging literature suggests the efficacy of antiangiogenic therapy,

particularly bevacizumab, for recurrent high-grade gliomas [157, 158].

Radioimmunotherapy. Locoregional radioimmunotherapy (RIT) have been proposed for targeting brain tumors. Monoclonal antibodies (MoAb) conjugated with high-energy β^- emitters (^{131}I, ^{90}Y or ^{177}Lu) are used for this purpose. Tumor cells that do not express the antigen on their surface can be damaged by the "cross-fire effect" [159]. Different strategies have been proposed to improve the tumor-to-non-tumor uptake ratio, such as the three-step pre-targeting radioimmunotherapy (pRIT) ("sandwich" approach) based on the avidin–biotin system, which has been employed with some success [160]. Disease-free survival in the treated patients was significantly longer than in patients undergoing conventional therapy [161]. Patients treated with pRIT and temozolomide have a significantly longer disease-free survival compared to patients treated with pRIT alone [162].

Differently from low aggressive forms of some tumors, such as thyroid cancer and prostate cancer, active surveillance does not represent a valid therapeutic approach for either high-grade or low-grade gliomas.

Meningiomas

Meningiomas are the most common benign intracranial tumors. Their prognosis is excellent, except when they are located in surgically inaccessible anatomical sites. Grade I meningiomas (also commonly referred to as typical meningiomas) have low proliferative rate [163]. Grade II meningiomas (i.e., atypical or anaplastic meningiomas that constitute less than 5% of all meningiomas) have histological features consistent with greater proliferative activity [164]. The recurrence rate after surgery is higher in grade II than in grade I meningiomas. All meningiomas are highly vascularized. Meningiomas express a wide range of receptors, which makes them sensitive to different hormonal controls and potential target for various radioligands. The diagnosis of meningiomas is easily performed on CT. The distinction between typical and atypical meningiomas is not reliable on either CT or MR, and the capacity of PET to predict grading and recurrence of disease has been tested. However, meningiomas located near the base of the skull may be difficult to distinguish from other lesions, such as lymphomas, metastases, or neurinomas [165], and ^{68}Ga-DOTATOC-PET data can complement anatomical data from MR and CT to improve target volume definition, especially in cases with complex infiltration and recurrent disease after surgery [166, 167].

CMR_{glc} is significantly higher in atypical meningiomas than in typical meningiomas and correlates with tumor proliferation rate [168–170]. However, remarkable differences in CMR_{glc} are observed among different types of typical meningiomas [168, 169]. Less frequently [^{18}F]FDG PET did not predict histological or behavioral features [171]. Multivariate analysis showed that, in addition to MIB-1 labeling index, presence of brain invasion, and WHO grade, [^{18}F]FDG uptake in meningiomas predicts tumor recurrence [170].

In addition to [^{18}F]FDG, several other tracers have been shown to accumulate in meningiomas, including [^{11}C]MET, [^{11}C]choline, and ^{18}F-FET. SUV_{max} of [^{11}C]MET but not [^{18}F]FDG was correlated with Ki-67 in meningioma cells [171]. [^{11}C]MET PET/CT can be used for the definition of the GTV delineation in fractionated stereotactic radiotherapy of skull base meningiomas. [^{11}C]MET PET images incorporation into stereotactic radiotherapy plan allowed better definition of the GTV [172] and may lead to changes (both reductions and increases) of the GTV in a significant number of cases [173]. [^{11}C]MET PET was used in the evaluation of the response to therapy with interferon-alpha and be useful for predicting the clinical response, for determining the length of the therapy and for adjusting of drug dosage [174].

Giovacchini et al. described the uptake of [^{11}C]choline in a small group of seven meningioma patients that were also studied with [^{18}F]FDG. The uptake of [^{11}C]choline but not of [^{18}F]FDG was higher in patients with grade II than in grade I meningiomas [114]. Other case reports were subsequently published [175, 176].

SPECT somatostatin receptor scintigraphy, namely, ^{111}In-octreotide, has been used successfully

in the past owing to the frequent overexpression of somatostatin receptors (SSTR) $SSTR_2$ in meningiomas [177]. However, owing to the widespread development of generator-based ^{68}Ga-conjugates, PET has substantially substituted SPECT. The three compounds most commonly used for PET imaging are ^{68}Ga-DOTATOC (^{68}Ga-DOTA-Tyr^3-octreotide), ^{68}Ga-DOTANOC ([^{68}Ga]-DOTA-Nal^3-octreotide), and ^{68}Ga-DOTATATE (^{68}Ga-DOTA-Tyr^3-octreotate). ^{68}Ga-DOTATOC and ^{68}Ga-DOTATATE have high affinity for $SSTR_2$, which is the most common SSTR subtype found in meningiomas. ^{68}Ga-DOTANOC targets a broader range of somatostatin subtype receptors, including $SSTR_2$, $SSTR_3$, and $SSTR_5$ [178]. Initial studies were performed using ^{68}Ga-DOTANOC [179, 180]. Cumbersome kinetic analysis using the plasma input function was adopted [180]. An interesting study performed in an animal model kinetic analysis using the Logan graphical method was used to compute the distribution volume of the three tracers. Although the distribution volume was relatively similar with ^{68}Ga-DOTATATE and ^{68}Ga-DOTATOC, uptake was higher with ^{68}Ga-DOTATATE in the tumor than with ^{68}Ga-DOTANOC and ^{68}Ga-DOTATOC, suggesting a higher diagnostic value of ^{68}Ga-DOTATATE for detecting meningiomas [165]. Later studies have the visibility of qualitative and semiquantitative evaluation for routine clinical questions [181].

16α-^{18}F-fluoro-17β-oestradiol (^{18}F-FES) has been occasionally used to evaluate estrogenic receptors in meningiomas. The identification of meningiomas occurs in about 60% of cases [182].

Conclusion

Several traditional and new tracers have been developed for evaluating brain tumors. This abundance in radiopharmaceuticals together with the technical development of PET/CT tomographs first and then PET/MR has enabled a substantial deepening in the knowledge of morphological and functional properties of brain tumors. PET/MR scanners also have substantial logistic and technical advantages: one single imaging session can be performed for the individual patient ("one-stop-shop") and optimal technical conditions (minimization of movement, accurate coregistration) can be achieved.

Several studies on genetic predisposition and on the corresponding molecular pathology were also performed yielding important information on the pathophysiology and risk factors for brain tumors. Surgery still represents the cornerstone of therapy in gliomas, while the role of radiotherapy is increasing and combinations, with or without escalation, with temozolomide are being tested. Angiogenesis inhibitors, such as the monoclonal antibody bevacizumab, have been tested with promising results.

There are different clinical settings in which PET can be used in the clinical practice. The most frequent is the differential diagnosis between tumor recurrence and radiation injury, where radiological techniques including MR suffer substantially from both sensitivity and specificity. PET, especially in combination with MR, is increasingly more used for the definition of the gross tumor volume to be irradiated. The identification of the metabolically active volume can also be used to direct biopsy, for planning surgery, or can clarify an undetermined finding on MR. A unique capability of PET is to predict in vivo tumor grading better than any other technique. Generally, high metabolic activity is predictive of higher tumor grade, even though there is variable accuracy among tracers in such prediction; for example, [^{18}F]FDG is more accurate than amino acid tracers. Changes in cerebral tracer uptake can be monitored in response to therapy. Changes after therapy as well as baseline values in untreated patients have prognostic value.

Several radiopharmaceuticals have been developed to explore biochemical processes other than glucose metabolism that are associated to tumor growth. Amino acid tracers are sensitive to transport across the BBB and, to some extent, protein synthesis. Contrary to [^{18}F]FDG, amino acids are less involved in inflammation and therefore have higher specificity for differentiating tumor recurrence versus radiation necrosis. Among available tracers, [^{11}C]MET is the one that is nowadays more validated in the clinical setting and more

widely used. Other promising tracers include [^{18}F]FDOPA and ^{18}F-FET. However, the tumor uptake of [^{18}F]FDG has prognostic value. Other tracers, such as hypoxia tracers and radiolabeled choline, presently have a more uncertain role in the clinical routine, even though some interesting results derived from clinical research studies.

References

1. Ostrom QT, et al. CBTRUS statistical report: primary brain and central nervous system tumors diagnosed in the United States in 2006–2010. Neuro Oncol. 2013; 15 Suppl 2:ii1–56.
2. Wohrer A, et al. The Austrian brain tumour registry: a cooperative way to establish a population-based brain tumour registry. J Neurooncol. 2009;95(3):401–11.
3. Ostrom QT, et al. CBTRUS statistical report: primary brain and central nervous system tumors diagnosed in the United States in 2007–2011. Neuro Oncol. 2014; 16 Suppl 4:iv1–63.
4. DeAngelis LM. Brain tumors. N Engl J Med. 2001; 344(2):114–23.
5. Ohgaki H, Kleihues P. Population-based studies on incidence, survival rates, and genetic alterations in astrocytic and oligodendroglial gliomas. J Neuropathol Exp Neurol. 2005;64(6):479–89.
6. Central Nervous System. In: Edge DRBSB, Compton CC, Fritz AG, Greene FL, Trotti A, Moffi HL, editors. AJCC cancer staging manual. New York: Springer; 2010. p. 591–7.
7. Herholz K, et al. Brain tumors. Semin Nucl Med. 2012;42(6):356–70.
8. McLendon RE, Halperin EC. Is the long-term survival of patients with intracranial glioblastoma multiforme overstated? Cancer. 2003;98(8):1745–8.
9. Vigneswaran K, Neill S, Hadjipanayis CG. Beyond the World Health Organization grading of infiltrating gliomas: advances in the molecular genetics of glioma classification. Ann Transl Med. 2015;3(7):95.
10. Kraus JA, et al. Molecular genetic alterations in glioblastomas with oligodendroglial component. Acta Neuropathol. 2001;101(4):311–20.
11. Louis DN, et al. The 2007 WHO classification of tumours of the central nervous system. Acta Neuropathol. 2007;114(2):97–109.
12. Lau EW, et al. Comparative PET study using F-18 FET and F-18 FDG for the evaluation of patients with suspected brain tumour. J Clin Neurosci. 2010;17(1): 43–9.
13. Thompson L, Dong Y, Evans L. Chronic hypoxia increases inducible NOS-derived nitric oxide in fetal guinea pig hearts. Pediatr Res. 2009;65(2):188–92.
14. Barker 2nd FG, et al. Necrosis as a prognostic factor in glioblastoma multiforme. Cancer. 1996;77(6): 1161–6.
15. Weller M, et al. Molecular neuro-oncology in clinical practice: a new horizon. Lancet Oncol. 2013;14(9): e370–9.
16. Hegi ME, et al. MGMT gene silencing and benefit from temozolomide in glioblastoma. N Engl J Med. 2005;352(10):997–1003.
17. Mabray MC, Barajas Jr RF, Cha S. Modern brain tumor imaging. Brain Tumor Res Treat. 2015;3(1):8–23.
18. Mellinghoff IK, et al. Molecular determinants of the response of glioblastomas to EGFR kinase inhibitors. N Engl J Med. 2005;353(19):2012–24.
19. Sneed PK, et al. Large effect of age on the survival of patients with glioblastoma treated with radiotherapy and brachytherapy boost. Neurosurgery. 1995;36 (5):898–903; discussion 903–4.
20. Saconn PA, et al. Use of 3.0-T MRI for stereotactic radiosurgery planning for treatment of brain metastases: a single-institution retrospective review. Int J Radiat Oncol Biol Phys. 2010;78(4):1142–6.
21. Wen PY, et al. Updated response assessment criteria for high-grade gliomas: response assessment in neuro-oncology working group. J Clin Oncol. 2010; 28(11):1963–72.
22. Hilario A, et al. A prognostic model based on preoperative MRI predicts overall survival in patients with diffuse gliomas. AJNR Am J Neuroradiol. 2014; 35(6):1096–102.
23. Anger HO. Medical radioisotope scanning. Vienna: IAEA; 1959.
24. Strauss HW, et al. Nuclear cerebral angiography. Usefulness in the differential diagnosis of cerebrovascular disease and tumor. Arch Intern Med. 1973;131(2): 211–6.
25. Kaplan WD, et al. Thallium-201 brain tumor imaging: a comparative study with pathologic correlation. J Nucl Med. 1987;28(1):47–52.
26. Ancri D, et al. Diagnosis of cerebral lesions by Thallium 201. Radiology. 1978;128(2):417–22.
27. Biersack HJ, Grunwald F, Kropp J. Single photon emission computed tomography imaging of brain tumors. Semin Nucl Med. 1991;21(1):2–10.
28. Ishibashi M, et al. Thallium-201 in brain tumors: relationship between tumor cell activity in astrocytic tumor and proliferating cell nuclear antigen. J Nucl Med. 1995;36(12):2201–6.
29. Ciarmiello A, et al. Tumor clearance of technetium 99m-sestamibi as a predictor of response to neoadjuvant chemotherapy for locally advanced breast cancer. J Clin Oncol. 1998;16(5):1677–83.
30. Benard F, Romsa J, Hustinx R. Imaging gliomas with positron emission tomography and single-photon emission computed tomography. Semin Nucl Med. 2003;33(2):148–62.
31. Yokogami K, et al. Application of SPET using technetium-99m sestamibi in brain tumours and comparison with expression of the MDR-1 gene: is it possible to predict the response to chemotherapy in patients with gliomas by means of 99mTc-sestamibi SPET? Eur J Nucl Med. 1998;25(4):401–9.

32. Vaalburg W, et al. P-glycoprotein activity and biological response. Toxicol Appl Pharmacol. 2005;207 (2 Suppl):257–60.
33. Jacquier-Sarlin MR, Polla BS, Slosman DO. Oxidoreductive state: the major determinant for cellular retention of technetium-99m-HMPAO. J Nucl Med. 1996;37(8):1413–6.
34. Jacquier-Sarlin MR, Polla BS, Slosman DO. Cellular basis of ECD brain retention. J Nucl Med. 1996;37 (10):1694–7.
35. Langen KJ, et al. Tomographic studies of rCBF with [^{99m}Tc]-HM-PAO SPECT in patients with brain tumors: comparison with $C^{15}O_2$ continuous inhalation technique and PET. J Cereb Blood Flow Metab. 1988;8(6):S90–4.
36. Suess E, et al. Technetium-99m-d,l-hexamethylpropyleneamine oxime (HMPAO) uptake and glutathione content in brain tumors. J Nucl Med. 1991;32(9):1675–81.
37. Papazyan JP, et al. Discrepancies between HMPAO and ECD SPECT imaging in brain tumors. J Nucl Med. 1997;38(4):592–6.
38. Di Chiro G. Brain imaging of glucose utilization in cerebral tumors. Res Publ Assoc Res Nerv Ment Dis. 1985;63:185–97.
39. Sokoloff L, et al. The [^{14}C]deoxyglucose method for the measurement of local cerebral glucose utilization: theory, procedure, and normal values in the conscious and anesthetized albino rat. J Neurochem. 1977;28(5):897–916.
40. Varrone A, et al. EANM procedure guidelines for PET brain imaging using [^{18}F]FDG, version 2. Eur J Nucl Med Mol Imaging. 2009;36(12):2103–10.
41. Huang SC, et al. Error sensitivity of fluorodeoxyglucose method for measurement of cerebral metabolic rate of glucose. J Cereb Blood Flow Metab. 1981;1(4):391–401.
42. Di Chiro G, et al. Glucose utilization of cerebral gliomas measured by [^{18}F] fluorodeoxyglucose and positron emission tomography. Neurology. 1982;32(12):1323–9.
43. Patronas NJ, et al. Glycolytic rate (PET) and contrast enhancement (CT) in human cerebral gliomas. AJNR Am J Neuroradiol. 1983;4(3):533–5.
44. Delbeke D, et al. Optimal cutoff levels of F-18 fluorodeoxyglucose uptake in the differentiation of low-grade from high-grade brain tumors with PET. Radiology. 1995;195(1):47–52.
45. DeLaPaz RL, et al. Positron emission tomographic study of suppression of gray-matter glucose utilization by brain tumors. AJNR Am J Neuroradiol. 1983; 4(3):826–9.
46. Patronas NJ, et al. Depressed cerebellar glucose metabolism in supratentorial tumors. Brain Res. 1984;291(1):93–101.
47. Di Chiro G, Brooks RA. PET-FDG of untreated and treated cerebral gliomas. J Nucl Med. 1988; 29(3):421–3.
48. Tyler JL, et al. Metabolic and hemodynamic evaluation of gliomas using positron emission tomography. J Nucl Med. 1987;28(7):1123–33.
49. Piert M, et al. Diminished glucose transport and phosphorylation in Alzheimer's disease determined by dynamic FDG-PET. J Nucl Med. 1996;37(2):201–8.
50. Schmidt K, et al. Errors introduced by tissue heterogeneity in estimation of local cerebral glucose utilization with current kinetic models of the [18F] fluorodeoxyglucose method. J Cereb Blood Flow Metab. 1992;12(5):823–34.
51. Mazziotta JC, et al. Quantitation in positron emission computed tomography: 5 physical – anatomical effects. J Comput Assist Tomogr. 1981;5(5):734–43.
52. Di Chiro G, Brooks RA. PET quantitation: blessing and curse. J Nucl Med. 1988;29(9):1603–4.
53. Padma MV, et al. Prediction of pathology and survival by FDG PET in gliomas. J Neurooncol. 2003;64(3): 227–37.
54. Levivier M, et al. The integration of metabolic imaging in stereotactic procedures including radiosurgery: a review. J Neurosurg. 2002;97(5 Suppl):542–50.
55. Segtnan EA, et al. F-Fluorodeoxyglucose PET/computed tomography for primary brain tumors. PET Clin. 2015;10(1):59–73.
56. Ishizu K, et al. Effects of hyperglycemia on FDG uptake in human brain and glioma. J Nucl Med. 1994;35(7):1104–9.
57. Ishizu K, et al. Enhanced detection of brain tumors by [^{18}F]fluorodeoxyglucose PET with glucose loading. J Comput Assist Tomogr. 1994;18(1):12–5.
58. Spence AM, et al. ^{18}F-FDG PET of gliomas at delayed intervals: improved distinction between tumor and normal gray matter. J Nucl Med. 2004; 45(10):1653–9.
59. Henze M, et al. Detection of tumour progression in the follow-up of irradiated low-grade astrocytomas: comparison of 3-[^{123}I]iodo-alpha-methyl- L-tyrosine and ^{99m}Tc-MIBI SPET. Eur J Nucl Med Mol Imaging. 2002;29(11):1455–61.
60. Patronas NJ, et al. Work in progress: [^{18}F]fluorodeoxyglucose and positron emission tomography in the evaluation of radiation necrosis of the brain. Radiology. 1982;144(4):885–9.
61. Rozental JM, et al. Early changes in tumor metabolism after treatment: the effects of stereotactic radiotherapy. Int J Radiat Oncol Biol Phys. 1991;20(5):1053–60.
62. Pirotte B, et al. PET in stereotactic conditions increases the diagnostic yield of brain biopsy. Stereotact Funct Neurosurg. 1994;63(1–4):144–9.
63. Tralins KS, et al. Volumetric analysis of ^{18}F-FDG PET in glioblastoma multiforme: prognostic information and possible role in definition of target volumes in radiation dose escalation. J Nucl Med. 2002;43(12): 1667–73.
64. Douglas JG, et al. [F-18]-fluorodeoxyglucose positron emission tomography for targeting radiation dose escalation for patients with glioblastoma multiforme: clinical outcomes and patterns of failure. Int J Radiat Oncol Biol Phys. 2006;64(3):886–91.
65. Singhal T, et al. ^{11}C-L-methionine positron emission tomography in the clinical management of cerebral gliomas. Mol Imaging Biol. 2008;10(1):1–18.

66. Herholz K, Coope D, Jackson A. Metabolic and molecular imaging in neuro-oncology. Lancet Neurol. 2007;6(8):711–24.
67. van Waarde A, et al. Comparison of sigma-ligands and metabolic PET tracers for differentiating tumor from inflammation. J Nucl Med. 2006;47(1):150–4.
68. Kubota R, et al. Methionine uptake by tumor tissue: a microautoradiographic comparison with FDG. J Nucl Med. 1995;36(3):484–92.
69. Utriainen M, et al. Evaluation of brain tumor metabolism with [^{11}C]choline PET and 1H-MRS. J Neurooncol. 2003;62(3):329–38.
70. De Witte O, et al. Positron emission tomography with injection of methionine as a prognostic factor in glioma. J Neurosurg. 2001;95(5):746–50.
71. Kim S, et al. ^{11}C-methionine PET as a prognostic marker in patients with glioma: comparison with 18F-FDG PET. Eur J Nucl Med Mol Imaging. 2005;32(1):52–9.
72. Pirotte B, et al. Integration of [^{11}C]methionine-positron emission tomographic and magnetic resonance imaging for image-guided surgical resection of infiltrative low-grade brain tumors in children. Neurosurgery. 2005;57(1 Suppl):128–39.
73. Pirotte B, et al. Positron emission tomography for the early postsurgical evaluation of pediatric brain tumors. Childs Nerv Syst. 2005;21(4):294–300.
74. Pirotte BJ, et al. Positron emission tomography-guided volumetric resection of supratentorial high-grade gliomas: a survival analysis in 66 consecutive patients. Neurosurgery. 2009;64(3):471–81.
75. Grosu AL, et al. Validation of a method for automatic image fusion (BrainLAB System) of CT data and ^{11}C-methionine-PET data for stereotactic radiotherapy using a LINAC: first clinical experience. Int J Radiat Oncol Biol Phys. 2003;56(5):1450–63.
76. Nariai T, et al. Usefulness of L-[methyl-^{11}C] methionine-positron emission tomography as a biological monitoring tool in the treatment of glioma. J Neurosurg. 2005;103(3):498–507.
77. Terakawa Y, et al. Diagnostic accuracy of ^{11}C-methionine PET for differentiation of recurrent brain tumors from radiation necrosis after radiotherapy. J Nucl Med. 2008;49(5):694–9.
78. Biersack HJ, et al. Imaging of brain tumors with L-3-[^{123}I]iodo-alpha-methyl tyrosine and SPECT. J Nucl Med. 1989;30(1):110–2.
79. Langen KJ, et al. SPECT studies of brain tumors with L-3-[^{123}I]iodo-alpha-methyl tyrosine: comparison with PET, ^{124}IMT and first clinical results. J Nucl Med. 1990;31(3):281–6.
80. Kuwert T, et al. Uptake of iodine-123-alpha-methyl tyrosine by gliomas and non-neoplastic brain lesions. Eur J Nucl Med. 1996;23(10):1345–53.
81. Weber W, et al. Fluorine-18-FDG PET and iodine-123-IMT SPECT in the evaluation of brain tumors. J Nucl Med. 1997;38(5):802–8.
82. Schmidt D, et al. 3-[^{123}I]Iodo-alpha-methyl-L-tyrosine uptake in cerebral gliomas: relationship to histological grading and prognosis. Eur J Nucl Med. 2001;28(7):855–61.
83. Weber WA, et al. Correlation between postoperative 3-[^{123}I]iodo-L-alpha-methyltyrosine uptake and survival in patients with gliomas. J Nucl Med. 2001;42(8):1144–50.
84. Pauleit D, et al. Comparison of *O*-(2-^{18}F-fluoroethyl)-L-tyrosine PET and 3-^{123}I-iodo-alpha-methyl-L-tyrosine SPECT in brain tumors. J Nucl Med. 2004;45(3):374–81.
85. Gotz L, et al. PET and SPECT for radiation treatment planning. Q J Nucl Med Mol Imaging. 2012;56(2):163–72.
86. Dunet V, Prior JL. FET PET in neuro-oncology and in evaluation of treatment response. PET Clin. 2013;8:147–62.
87. Pauleit D, et al. Whole-body distribution and dosimetry of *O*-(2-[^{18}F]fluoroethyl)-L-tyrosine. Eur J Nucl Med Mol Imaging. 2003;30(4):519–24.
88. Weber WA, et al. *O*-(2-[^{18}F]fluoroethyl)-L-tyrosine and L-[methyl-^{11}C]methionine uptake in brain tumours: initial results of a comparative study. Eur J Nucl Med. 2000;27(5):542–9.
89. Wester HJ, et al. Synthesis and radiopharmacology of *O*-(2-[^{18}F]fluoroethyl)-L-tyrosine for tumor imaging. J Nucl Med. 1999;40(1):205–12.
90. Heiss P, et al. Investigation of transport mechanism and uptake kinetics of *O*-(2-[^{18}F]fluoroethyl)-L-tyrosine in vitro and in vivo. J Nucl Med. 1999;40(8):1367–73.
91. Langen KJ, et al. Comparison of fluorotyrosines and methionine uptake in F98 rat gliomas. Nucl Med Biol. 2003;30(5):501–8.
92. Dunet V, et al. Performance of ^{18}F-fluoro-ethyl-tyrosine (^{18}F-FET) PET for the differential diagnosis of primary brain tumor: a systematic review and meta analysis. J Nucl Med. 2012;53(2):207–14.
93. Vander Borght T, et al. EANM procedure guidelines for brain tumour imaging using labelled amino acid analogues. Eur J Nucl Med Mol Imaging. 2006;33(11):1374–80.
94. Pauleit D, et al. Comparison of ^{18}F-FET and ^{18}F-FDG PET in brain tumors. Nucl Med Biol. 2009;36(7):779–87.
95. Jeong SY, Lim SM. Comparison of 3′-deoxy-3′-[^{18}F] fluorothymidine PET and *O*-(2-[^{18}F]fluoroethyl)-L-tyrosine PET in patients with newly diagnosed glioma. Nucl Med Biol. 2012;39(7):977–81.
96. Roelcke U, et al. F-18 choline PET does not detect increased metabolism in F-18 fluoroethyltyrosine-negative low-grade gliomas. Clin Nucl Med. 2012;37(1):e1–3.
97. Calcagni ML, et al. Dynamic *O*-(2-[^{18}F]fluoroethyl)-L-tyrosine (F-18 FET) PET for glioma grading: assessment of individual probability of malignancy. Clin Nucl Med. 2011;36(10):841–7.

98. Jansen NL, et al. MRI-suspected low-grade glioma: is there a need to perform dynamic FET PET? Eur J Nucl Med Mol Imaging. 2012;39(6):1021–9.
99. Pyka T, et al. Prediction of glioma recurrence using dynamic ^{18}F-fluoroethyltyrosine PET. AJNR Am J Neuroradiol. 2014;35(10):1924–9.
100. Becherer A, et al. Brain tumour imaging with PET: a comparison between [^{18}F]fluorodopa and [^{11}C]methionine. Eur J Nucl Med Mol Imaging. 2003;30(11):1561–7.
101. Talbot JN, et al. FDOPA PET has clinical utility in brain tumour imaging: a proposal for a revision of the recent EANM guidelines. Eur J Nucl Med Mol Imaging. 2007;34(7):1131–2; author reply 1133–4.
102. Karunanithi S, et al. ^{18}F-FDOPA PET/CT for detection of recurrence in patients with glioma: prospective comparison with ^{18}F-FDG PET/CT. Eur J Nucl Med Mol Imaging. 2013;40(7):1025–35.
103. Tripathi M, et al. Comparative evaluation of F-18 FDOPA, F-18 FDG, and F-18 FLT-PET/CT for metabolic imaging of low grade gliomas. Clin Nucl Med. 2009;34(12):878–83.
104. Shields AF, et al. Cellular sources of thymidine nucleotides: studies for PET. J Nucl Med. 1987;28(9):1435–40.
105. Mankoff DA, et al. Kinetic analysis of 2-[carbon-11] thymidine PET imaging studies: compartmental model and mathematical analysis. J Nucl Med. 1998;39(6):1043–55.
106. Grierson JR, et al. Metabolism of 3′-deoxy-3′-[F-18] fluorothymidine in proliferating A549 cells: validations for positron emission tomography. Nucl Med Biol. 2004;31(7):829–37.
107. Muzi M, et al. Kinetic analysis of 3′-deoxy-3′-^{18}F-fluorothymidine in patients with gliomas. J Nucl Med. 2006;47(10):1612–21.
108. Ullrich R, et al. Glioma proliferation as assessed by 3′-fluoro-3′-deoxy-L-thymidine positron emission tomography in patients with newly diagnosed high-grade glioma. Clin Cancer Res. 2008;14(7):2049–55.
109. Fink J, et al. Multi-modality brain tumor imaging – MRI, PET, and PET/MRI. J Nucl Med. 2015;56:1554–61.
110. Chen W, et al. Predicting treatment response of malignant gliomas to bevacizumab and irinotecan by imaging proliferation with [^{18}F]fluorothymidine positron emission tomography: a pilot study. J Clin Oncol. 2007;25(30):4714–21.
111. Hatakeyama T, et al. 11C-methionine (MET) and ^{18}F-fluorothymidine (FLT) PET in patients with newly diagnosed glioma. Eur J Nucl Med Mol Imaging. 2008;35(11):2009–17.
112. Grosu AL, et al. Positron emission tomography for radiation treatment planning. Strahlenther Onkol. 2005;181(8):483–99.
113. Huang Z, et al. Misdiagnoses of ^{11}C-choline combined with ^{18}F-FDG PET imaging in brain tumours. Nucl Med Commun. 2008;29(4):354–8.
114. Giovacchini G, et al. C-11 choline versus F-18 fluorodeoxyglucose for imaging meningiomas: an initial experience. Clin Nucl Med. 2009;34(1):7–10.
115. Hara T, et al. Use of ^{18}F-choline and ^{11}C-choline as contrast agents in positron emission tomography imaging-guided stereotactic biopsy sampling of gliomas. J Neurosurg. 2003;99(3):474–9.
116. Ohtani T, et al. Brain tumour imaging with carbon-11 choline: comparison with FDG PET and gadolinium-enhanced MR imaging. Eur J Nucl Med. 2001;28(11):1664–70.
117. Li FM, et al. ^{11}C-CHO PET in optimization of target volume delineation and treatment regimens in postoperative radiotherapy for brain gliomas. Nucl Med Biol. 2012;39(3):437–42.
118. Kato T, et al. Metabolic assessment of gliomas using ^{11}C-methionine, [^{18}F]fluorodeoxyglucose, and ^{11}C-choline positron-emission tomography. AJNR Am J Neuroradiol. 2008;29(6):1176–82.
119. Li W, et al. ^{11}C-choline PET/CT tumor recurrence detection and survival prediction in post-treatment patients with high-grade gliomas. Tumour Biol. 2014;35(12):12353–60.
120. Tan H, et al. Comparison of MRI, F-18 FDG, and ^{11}C-choline PET/CT for their potentials in differentiating brain tumor recurrence from brain tumor necrosis following radiotherapy. Clin Nucl Med. 2011;36(11):978–81.
121. Markus R, et al. Statistical parametric mapping of hypoxic tissue identified by [^{18}F]fluoromisonidazole and positron emission tomography following acute ischemic stroke. Neuroimage. 2002;16(2):425–33.
122. Valk PE, et al. Hypoxia in human gliomas: demonstration by PET with fluorine-18-fluoromisonidazole. J Nucl Med. 1992;33(12):2133–7.
123. Grunbaum Z, et al. Synthesis and characterization of congeners of misonidazole for imaging hypoxia. J Nucl Med. 1987;28(1):68–75.
124. Bruehlmeier M, et al. Assessment of hypoxia and perfusion in human brain tumors using PET with ^{18}F-fluoromisonidazole and ^{15}O-H_2O. J Nucl Med. 2004;45(11):1851–9.
125. Swanson KR, et al. Complementary but distinct roles for MRI and ^{18}F-fluoromisonidazole PET in the assessment of human glioblastomas. J Nucl Med. 2009;50(1):36–44.
126. Hirata K, et al. ^{18}F-Fluoromisonidazole positron emission tomography may differentiate glioblastoma multiforme from less malignant gliomas. Eur J Nucl Med Mol Imaging. 2012;39(5):760–70.
127. Werner P, et al. Current status and future role of brain PET/MRI in clinical and research settings. Eur J Nucl Med Mol Imaging. 2015;42(3):512–26.
128. Catana C, et al. PET/MRI for neurologic applications. J Nucl Med. 2012;53(12):1916–25.
129. Charnley N, et al. Early change in glucose metabolic rate measured using FDG-PET in patients with high-grade glioma predicts response to temozolomide but

not temozolomide plus radiotherapy. Int J Radiat Oncol Biol Phys. 2006;66(2):331–8.
130. Boss A, et al. Hybrid PET/MRI of intracranial masses: initial experiences and comparison to PET/CT. J Nucl Med. 2010;51(8):1198–205.
131. Bisdas S, et al. Metabolic mapping of gliomas using hybrid MR-PET imaging: feasibility of the method and spatial distribution of metabolic changes. Invest Radiol. 2013;48(5):295–301.
132. Preuss M, et al. Integrated PET/MRI for planning navigated biopsies in pediatric brain tumors. Childs Nerv Syst. 2014;30(8):1399–403.
133. Garibotto V, et al. Molecular neuroimaging with PET/MRI. Clin Transl Imaging. 2013;1(1):53–63.
134. Dunet V, et al. Combination of MRI and dynamic FET PET for initial glioma grading. Nuklearmedizin. 2014;53(4):155–61.
135. Lustig RA, et al. Imaging response in malignant glioma, RTOG 90–06. Am J Clin Oncol. 2007;30(1): 32–7.
136. Patronas NJ, et al. Prediction of survival in glioma patients by means of positron emission tomography. J Neurosurg. 1985;62(6):816–22.
137. Alavi JB, et al. Positron emission tomography in patients with glioma. A predictor of prognosis. Cancer. 1988;62(6):1074–8.
138. Santra A, et al. F-18 FDG PET-CT for predicting survival in patients with recurrent glioma: a prospective study. Neuroradiology. 2011;53(12):1017–24.
139. Colavolpe C, et al. FDG-PET predicts survival in recurrent high-grade gliomas treated with bevacizumab and irinotecan. Neuro Oncol. 2012; 14(5):649–57.
140. Colavolpe C, et al. Independent prognostic value of pre-treatment 18-FDG-PET in high-grade gliomas. J Neurooncol. 2012;107(3):527–35.
141. Brock CS, et al. Early evaluation of tumour metabolic response using [^{18}F]fluorodeoxyglucose and positron emission tomography: a pilot study following the phase II chemotherapy schedule for temozolomide in recurrent high-grade gliomas. Br J Cancer. 2000;82(3):608–15.
142. Hillner BE, et al. Impact of dedicated brain PET on intended patient management in participants of the national oncologic PET registry. Mol Imaging Biol. 2011;13(1):161–5.
143. Floeth FW, et al. Prognostic value of *O*-(2-^{18}F-fluoroethyl)-L-tyrosine PET and MRI in low-grade glioma. J Nucl Med. 2007;48(4):519–27.
144. Piroth MD, et al. Prognostic impact of postoperative, pre-irradiation ^{18}F-fluoroethyl-l-tyrosine uptake in glioblastoma patients treated with radiochemotherapy. Radiother Oncol. 2011;99(2):218–24.
145. Hutterer M, et al. *O*-(2-^{18}F-fluoroethyl)-L-tyrosine PET predicts failure of antiangiogenic treatment in patients with recurrent high-grade glioma. J Nucl Med. 2011;52(6):856–64.
146. Galldiks N, et al. Assessment of treatment response in patients with glioblastoma using *O*-(2-^{18}F-fluoroethyl)-L-tyrosine PET in comparison to MRI. J Nucl Med. 2012;53(7):1048–57.
147. Harris RJ, et al. ^{18}F-FDOPA and ^{18}F-FLT positron emission tomography parametric response maps predict response in recurrent malignant gliomas treated with bevacizumab. Neuro Oncol. 2012;14(8): 1079–89.
148. Schwarzenberg J, et al. Treatment response evaluation using ^{18}F-FDOPA PET in patients with recurrent malignant glioma on bevacizumab therapy. Clin Cancer Res. 2014;20(13):3550–9.
149. Mariani G, et al. A review on the clinical uses of SPECT/CT. Eur J Nucl Med Mol Imaging. 2010;37 (10):1959–85.
150. Buck AK, et al. SPECT/CT. J Nucl Med. 2008;49(8): 1305–19.
151. Hayashi M, et al. Comparison of methods of attenuation and scatter correction in brain perfusion SPECT. J Nucl Med Technol. 2005;33(4):224–9.
152. Filippi L, et al. Usefulness of SPECT/CT with a hybrid camera for the functional anatomical mapping of primary brain tumors by [Tc99m] tetrofosmin. Cancer Biother Radiopharm. 2006;21(1):41–8.
153. Schillaci O, et al. Single-photon emission computed tomography/computed tomography in brain tumors. Semin Nucl Med. 2007;37(1):34–47.
154. Kortmann RD. Radiotherapy in low-grade gliomas: pros. Semin Oncol. 2003;30(6 Suppl 19):29–33.
155. van den Bent MJ, et al. Phase II study of first-line chemotherapy with temozolomide in recurrent oligodendroglial tumors: the European Organization for Research and Treatment of Cancer Brain Tumor Group Study 26971. J Clin Oncol. 2003;21(13): 2525–8.
156. Glas M, et al. Long-term survival of patients with glioblastoma treated with radiotherapy and lomustine plus temozolomide. J Clin Oncol. 2009;27(8):1257–61.
157. Olson JJ, et al. The role of cytotoxic chemotherapy in the management of progressive glioblastoma: a systematic review and evidence-based clinical practice guideline. J Neurooncol. 2014;118(3):501–55.
158. Chamberlain MC, Raizer J. Antiangiogenic therapy for high-grade gliomas. CNS Neurol Disord Drug Targets. 2009;8(3):184–94.
159. Mariani G, Kassis AI, Adelstein SJ. Antibody internalization by tumor cells: implications for tumor diagnosis and therapy. J Nucl Med Allied Sci. 1990;34(1): 51–4.
160. Paganelli G, et al. Three-step monoclonal antibody tumor targeting in carcinoembryonic antigen-positive patients. Cancer Res. 1991;51(21):5960–6.
161. Grana C, et al. Pretargeted adjuvant radioimmunotherapy with yttrium-90-biotin in malignant glioma patients: a pilot study. Br J Cancer. 2002;86 (2):207–12.
162. Bartolomei M, et al. Combined treatment of glioblastoma patients with locoregional pre-targeted ^{90}Y-biotin radioimmunotherapy and temozolomide. Q J Nucl Med Mol Imaging. 2004;48(3):220–8.

163. Sekhar LN, Levine ZT, Sarma S. Grading of meningiomas. J Clin Neurosci. 2001;8 Suppl 1:1–7.
164. Johnson MD, et al. New prospects for management and treatment of inoperable and recurrent skull base meningiomas. J Neurooncol. 2008;86(1):109–22.
165. Soto-Montenegro ML, et al. Meningiomas: a comparative study of ^{68}Ga-DOTATOC, ^{68}Ga-DOTANOC and ^{68}Ga-DOTATATE for molecular imaging in mice. PLoS One. 2014;9(11):e111624.
166. Milker-Zabel S, et al. Improved target volume definition for fractionated stereotactic radiotherapy in patients with intracranial meningiomas by correlation of CT, MRI, and [^{68}Ga]-DOTATOC-PET. Int J Radiat Oncol Biol Phys. 2006;65(1):222–7.
167. Afshar-Oromieh A, et al. Detection of cranial meningiomas: comparison of ^{68}Ga-DOTATOC PET/CT and contrast-enhanced MRI. Eur J Nucl Med Mol Imaging. 2012;39(9):1409–15.
168. Di Chiro G, et al. Glucose utilization by intracranial meningiomas as an index of tumor aggressivity and probability of recurrence: a PET study. Radiology. 1987;164(2):521–6.
169. Lippitz B, et al. PET-study of intracranial meningiomas: correlation with histopathology, cellularity and proliferation rate. Acta Neurochir Suppl. 1996;65:108–11.
170. Lee JW, et al. ^{18}F-FDG PET in the assessment of tumor grade and prediction of tumor recurrence in intracranial meningioma. Eur J Nucl Med Mol Imaging. 2009;36:1574–82.
171. Iuchi T, et al. Glucose and methionine uptake and proliferative activity in meningiomas. Neurol Res. 1999;21(7):640–4.
172. Grosu AL, et al. ^{11}C-methionine PET improves the target volume delineation of meningiomas treated with stereotactic fractionated radiotherapy. Int J Radiat Oncol Biol Phys. 2006;66(2):339–44.
173. Astner ST, et al. Effect of ^{11}C-methionine-positron emission tomography on gross tumor volume delineation in stereotactic radiotherapy of skull base meningiomas. Int J Radiat Oncol Biol Phys. 2008;72(4):1161–7.
174. Muhr C, et al. Meningioma treated with interferon-alpha, evaluated with [^{11}C]-L-methionine positron emission tomography. Clin Cancer Res. 2001;7(8):2269–76.
175. Bertagna F, et al. Incidental ^{11}C-choline PET/CT brain uptake due to meningioma in a patient studied for prostate cancer: correlation with MRI and imaging fusion. Clin Nucl Med. 2013;38(11):e435–7.
176. Calabria F, et al. A case of intracranial meningioma detected by ^{18}F-choline PET/CT and examined by PET/MRI fusion imaging. Rev Esp Med Nucl Imagen Mol. 2014;33(5):306–7.
177. Schulz S, et al. Immunohistochemical determination of five somatostatin receptors in meningioma reveals frequent overexpression of somatostatin receptor subtype sst2A. Clin Cancer Res. 2000;6(5):1865–74.
178. von Wild KR. New development of functional neurorehabilitation in neurosurgery. Acta Neurochir Suppl. 2003;87:43–7.
179. Henze M, et al. PET imaging of somatostatin receptors using [^{68}GA]DOTA-D-Phe^{1}-Tyr^{3}-octreotide: first results in patients with meningiomas. J Nucl Med. 2001;42(7):1053–6.
180. Henze M, et al. Characterization of ^{68}Ga-DOTA-D-Phe1-Tyr3-octreotide kinetics in patients with meningiomas. J Nucl Med. 2005;46(5):763–9.
181. Afshar-Oromieh A, et al. Comparison of ^{68}Ga-DOTATOC-PET/CT and PET/MRI hybrid systems in patients with cranial meningioma: initial results. Neuro Oncol. 2015;17(2):312–9.
182. Moresco RM, et al. Oestrogen receptors in meningiomas: a correlative PET and immunohistochemical study. Nucl Med Commun. 1997;18(7):606–15.
183. Chao ST, et al. The sensitivity and specificity of FDG PET in distinguishing recurrent brain tumor from radionecrosis in patients treated with stereotactic radiosurgery. Int J Cancer. 2001;96(3):191–7.
184. Nihashi T, Dahabreh IJ, Terasawa T. Diagnostic accuracy of PET for recurrent glioma diagnosis: a meta-analysis. AJNR Am J Neuroradiol. 2013;34(5):944–50, S1–11.
185. Choi SJ, et al. [^{18}F]3′-deoxy-3′-fluorothymidine PET for the diagnosis and grading of brain tumors. Eur J Nucl Med Mol Imaging. 2005;32(6):653–9.
186. Fallanca F, et al. Incidental detection by [^{11}C]choline PET/CT of meningiomas in prostate cancer patients. Q J Nucl Med Mol Imaging. 2009;53(4):417–21.